



1 **A Holocene history of climate, fire, landscape evolution, and human**  
2 **activity in Northeast Iceland**

3 Nicolò Ardenghi<sup>1</sup>, David J. Harning<sup>1</sup>, Jonathan H. Raberg<sup>1</sup>, Brooke R. Holman<sup>1</sup>, Thorvaldur Thordarson<sup>2</sup>,  
4 Áslaug Geirsdóttir<sup>2</sup>, Gifford H. Miller<sup>1,3</sup>, Julio Sepúlveda<sup>1,3</sup>

5 <sup>1</sup>Institute of Arctic and Alpine Research (INSTAAR), University of Colorado Boulder, CO, 80309, USA

6 <sup>2</sup>80309, Faculty of Earth Sciences, University of Iceland, Reykjavík, Iceland

7 <sup>3</sup>Department of Geological Sciences, University of Colorado Boulder, CO, USA

8 *Correspondence to:* Nicolò Ardenghi (nicolo.ardenghi@gmail.com)



9 **1 Abstract**

10 Paleoclimate reconstructions across Iceland provide a template for past changes in climate across the northern North Atlantic,  
11 a crucial region due to its position relative to the global northward heat transport system and its vulnerability to climate change.  
12 The roles of orbitally driven summer cooling, volcanism, and human impact as triggers of local environmental changes in the  
13 Holocene of Iceland, remain debated. While there are indications that human impact may have reduced environmental  
14 resilience during Late Holocene summer cooling, it is still difficult to resolve to what extent human and natural factors affected  
15 Iceland's Late Holocene landscape instability. Here, we present a continuous Holocene fire record of northeastern Iceland  
16 from proxies archived in Stóra Viðarvatn sediment. We use pyrogenic polycyclic aromatic hydrocarbons (pyroPAHs) to trace  
17 shifts in fire regimes, paired with continuous biomarker and bulk geochemical records of soil erosion, lake productivity, and  
18 human presence. The molecular composition of pyroPAHs and a wind pattern reconstruction indicate a naturally driven fire  
19 signal that is mostly regional. Generally low fire frequency during most of the Holocene significantly increased at 3 ka and  
20 again after 1.5 ka BP, before known human settlement in Iceland. We propose that shifts in vegetation type caused by cooling  
21 summers over the past 3 kyr, in addition to changes in atmospheric circulation, such as shifts in North Atlantic Oscillation  
22 (NAO) regime, led to increased aridity and biomass flammability. Our results show no evidence of faecal biomarkers  
23 associated with human activity during or after human colonisation in the 9<sup>th</sup> century CE. Instead, faecal biomarkers follow the  
24 pattern described by erosional proxies, pointing toward a negligible human presence and/or a diluted signal in the lake's  
25 catchment. However, low post-colonisation levels of pyroPAHs, in contrast to an increasing flux of erosional bulk proxies,  
26 suggest that farming and animal husbandry may have suppressed fire frequency by reducing the spread and flammability of  
27 fire-prone vegetation (e.g., heathlands).  
28 Overall, our results describe a fire frequency heavily influenced by long term changes in climate through the Holocene. They  
29 also suggest that human colonisation had contrasting effects on the local environment by lowering its resilience to soil erosion  
30 while increasing its resilience to fire.



31 **2 Introduction**

32 Iceland is highly sensitive to most mechanisms controlling the evolution of Holocene climate in the North Atlantic, from  
33 millennial (e.g., shifts in deep water formation and ocean current positions) to sub-decadal timescales (e.g., variability of the  
34 North Atlantic Oscillation) (Harning et al., 2021; Mjell et al., 2016; Moossen et al., 2015; Petit et al., 2020). Recent lake  
35 sedimentary records in Iceland (Alsos et al., 2021; Geirsdóttir et al., 2009a, 2013, 2019, 2020; Harning et al., 2016, 2020;  
36 Hiles et al., 2021; Larsen et al., 2011, 2012; Richter et al., 2021) draw a comprehensive picture of Icelandic environments  
37 during the Holocene (last 11.7 kyr). These Holocene paleoclimate reconstructions derived from lake sediments in Iceland show  
38 first-order millennial trends that reflect orbitally-driven changes in Northern Hemisphere summer insolation, and millennial to  
39 sub-millennial changes that are primarily impacted by northern North Atlantic ocean circulation and to a part by local  
40 volcanism (e.g., Flowers et al., 2008; Geirsdóttir et al., 2013, 2020; Harning et al., 2018b; Larsen et al., 2012). These Holocene  
41 climate reconstructions further indicate a major shift from occasional to increasingly severe landscape instability and soil  
42 erosion occurring at least 300 years before the acknowledged settlement of Iceland (ca 870 CE; The Book of Icelanders  
43 “Íslendigabók”, by Ari Thorgilsson, 12<sup>th</sup> century CE, e.g., Smith, 1995), suggesting that human impact had a secondary role  
44 to climate by lowering the resilience of the environment to an already ongoing naturally driven erosion (e.g., Bates et al., 2021;  
45 Geirsdóttir et al., 2009b, 2020). The ability to generate high-resolution Holocene terrestrial climate records, along with  
46 Iceland’s relatively short settlement history, makes Iceland an ideal location to attempt disentangling the impact of natural  
47 climate variability and human activities on the changes in the local landscape during the Late Holocene.

48 In this study, we use multiple organic proxies from a Holocene sediment core from the Stóra Viðarvatn lake in northeast  
49 Iceland to investigate the effects of natural and anthropogenic drivers on the local Icelandic environment. First, we focus on  
50 tracing the evolution of fire regimes using pyrogenic polycyclic aromatic hydrocarbons (pyroPAHs; Lima et al., 2005). Fires  
51 can have a significant impact on ecosystems, affecting vegetation patterns, nutrient cycling, and wildlife habitat (e.g.,  
52 Goldammer and Furyaev, 1996). The frequency, intensity, and spatial extent of fires can provide insights into past climate and  
53 environmental conditions (e.g., Marlon, 2009; Power et al., 2008) and, to our knowledge, there are no such records for the  
54 Holocene in Iceland, while limited data is available for the surrounding regions (Chen et al., 2023; Marlon et al., 2013; Segato  
55 et al., 2021; Zennaro et al., 2014). Second, as fire frequency can be influenced by human activities as well (e.g., Marlon et al.,  
56 2009, 2013; Zennaro et al., 2015), we also analyse faecal markers of human presence (Vázquez et al., 2021). By analysing  
57 these biomarkers from deglaciation to present, we can define their natural, pre-settlement background levels and thus  
58 potentially trace anthropogenic impact on the local environment, pinpointing human arrival in the lake catchment.

59 Finally, by coupling fire and human presence biomarker records with established proxies for environmental change (e.g., soil  
60 erosion and primary productivity, e.g., Argiriadis et al., 2018; Geirsdóttir et al., 2013; Gross, 2017), we test what control  
61 natural and/or human factors had on the evolution of the Holocene landscape in Iceland.

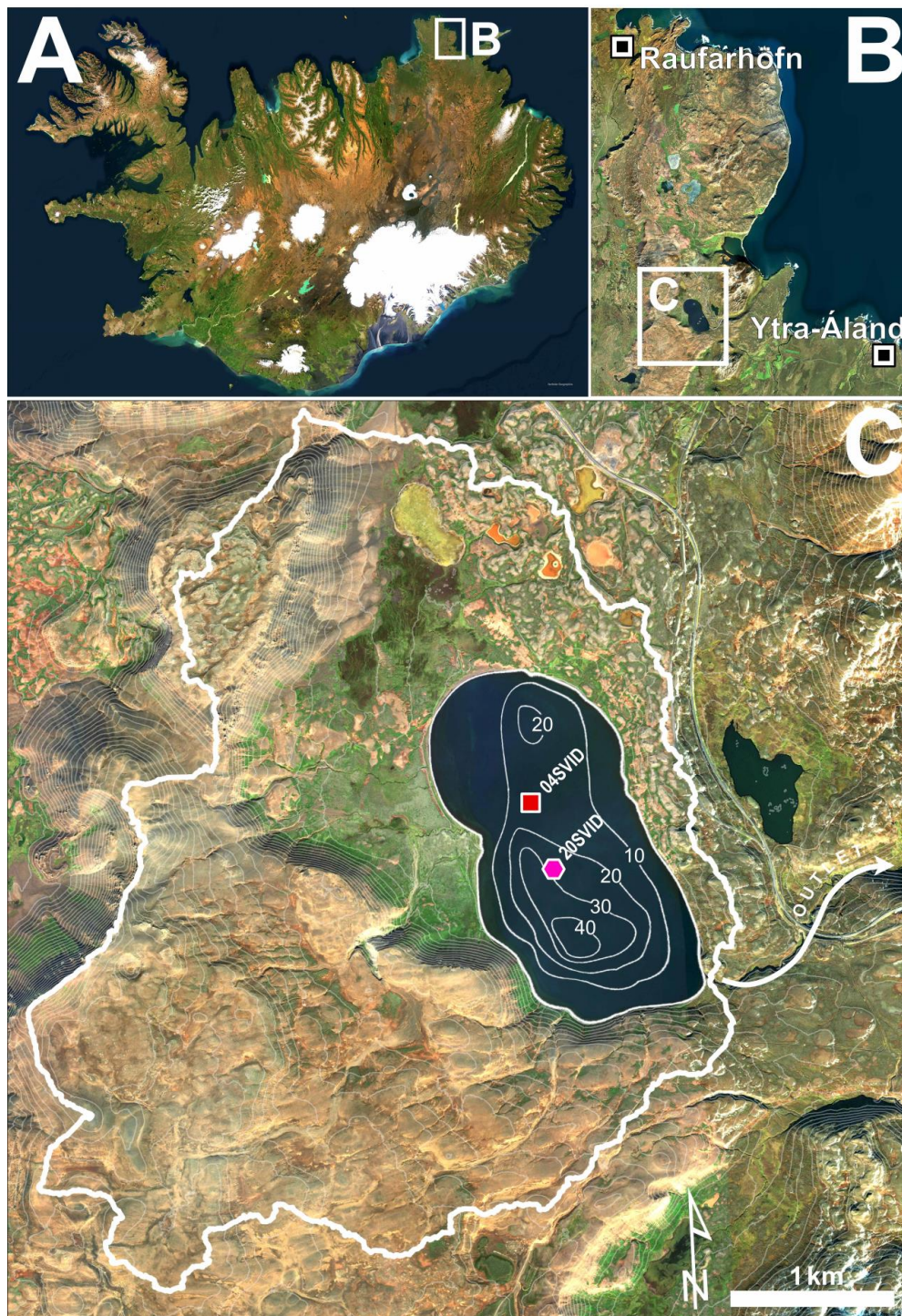


62 **3 Methods**

63 **3.1 Study site**

64 Stóra Viðarvatn (SVID) is a lake (2.6 km<sup>2</sup> surface area) located in NE Iceland (Fig. 1A-B) at an elevation of 151 m asl. SVID  
65 has a maximum depth of 48 m, a catchment area of 17 km<sup>2</sup> (including the lake surface), and a volume of ca 3.6×10<sup>7</sup> m<sup>3</sup> (this  
66 study, based on data from the National Land Survey of Iceland, Landmælingar Íslands, 2023; Axford et al., 2007). The nearby  
67 Raufarhöfn station (Icelandic Meteorological Office, 2022) provides weather data for the 1961–1990 CE interval: mean annual  
68 temperature is 2 °C with a maximum in July-August (8 °C), while the lake surface is usually frozen between November and  
69 March; mean annual precipitation is 733 mm a<sup>-1</sup> with lowest values occurring in May (28 mm) and the highest in October (ca  
70 86 mm), suggesting a lake-water residence time between five and nine years.

71 In February 2020, we recovered a 8.93 m long core 20-SVID-02 (66.236867° N; -15.837837° E; 1C) from 17.4 m water depth  
72 near the centre of the lake. Previously, two studies have analysed an 8 m long core (04-SVID-03; 1C) retrieved in February  
73 2004 to trace Holocene temperature (Axford et al., 2007) and δ<sup>18</sup>O from chironomid remains, as well as the δD, δ<sup>13</sup>C, δ<sup>15</sup>N of  
74 total organic matter (Wooller et al., 2008) at a 1–0.2 kyr resolution.



75

76 Figure 1: (A) Study area in NE Iceland; (B) Location of the Raufarhöfn climatological station and Ytra-Áland site (Karlsson et al., 2014), which are 20 km NNW and 13 km ESE from Stóra Viðarvatn (SVID), respectively; (C) Location and catchment area of  
77 the Stóra Viðarvatn lake: 20-SVID-02 core is marked by a pink hexagon and an older 04-SVID-03 core by a red square (Axford et al., 2007); SVID bathymetry (10 m isolines) is reported by Axford et al. (2007); watershed catchment and contour lines (10 m) are  
78 calculated via ArcGIS (Esri, 2023) based on digital elevation models provided by the National Land Survey of Iceland; basemap  
79 sourced from Esri.  
80  
81



## 82 3.2 Tephrochronology

83 Our sediment core chronology takes advantage of the geochemical fingerprints of visible Icelandic tephra layers and their  
84 correlation to marker tephra of known age. Thirteen tephra layers were sampled along the vertical axis, sieved to isolate glass  
85 fragments between 125 and 500  $\mu\text{m}$ , and embedded in epoxy plugs. At the University of Iceland, individual glass shards were  
86 analysed on a JEOL JXA-8230 electron microprobe using an acceleration voltage of 15 kV, beam current of 10 nA, and a  
87 beam diameter of 10  $\mu\text{m}$ . The international A99 standard was used to monitor for instrumental drift and maintain consistency  
88 between measurements. Tephra origin was then assessed using major oxide compositions, following the systematic procedures  
89 outlined in Jennings et al., 2014 and Harning et al., 2018a. Briefly, based on  $\text{SiO}_2$  wt% vs total alkali ( $\text{Na}_2\text{O} + \text{K}_2\text{O}$ ) wt%, we  
90 determined whether the tephra volcanic source is mafic (tholeiitic or alkalic), intermediate and/or rhyolitic. From here, we  
91 objectively discriminate the source volcanic system through a detailed series of bi-elemental plots produced from available  
92 compositional data on Icelandic tephra. Source eruption was then determined using the geochemical fingerprint and relevant  
93 stratigraphic information. See supplemental information for complete major oxide compositions and bi-elemental plots.  
94 Using the 13 marker tephra layers of known age (Table 1), we generated a Bayesian age model using the R package rbacon  
95 (Blaauw and Christen, 2011; R Core Team, 2020) and default model functions (Fig. 2). We used the ‘slumps’ function for the  
96 thicker tephra layers (e.g., Hekla 3 and Hekla 4) to reflect their instantaneous deposition on geologic timescales.

## 97 3.3 Sample preparation and analysis

98 At the University of Colorado Boulder, we retrieved a total of 196 sediment core samples at an average spacing of 4.5 cm,  
99 providing a temporal resolution of decadal to centennial time scales. We freeze-dried samples for 24–48 hours, and ground  
100 and homogenised them (mean weight 1.5 g, range 0.6–6.6 g) using an agate mortar and pestle. Using 13–70 mg of sediment,  
101 we measured total carbon (TC), total nitrogen (TN), and  $\delta^{13}\text{C}$  (relative to VPDB) on an elemental analyser linked to a Thermo  
102 Delta V isotope ratio mass spectrometer (EA-IRMS) in the Earth Systems Stable Isotope Laboratory at the University of  
103 Colorado Boulder; samples were analysed against a suite of secondary laboratory standards that are extensively calibrated to  
104 international standard reference materials to correct for size, blank-mixing, linearity and drift effects (Harning et al., 2018b).  
105 We analysed 9–11 mg of sediment for biogenic silica by Diffuse Reflectance Fourier Transform Infrared Spectrometry  
106 (FTIRS) on a Bruker Vertex 70 with a Praying Mantis diffuse reflectivity accessory (Harrick) and report values in FTIRS -  
107 Fourier Transform Infrared Spectroscopy absorbance units (e.g., Harning et al., 2018b).  
108 We processed 86 selected samples for organic biomarker analyses. We extracted 0.4–2 g of dry sediment with an accelerated  
109 solvent extractor (Dionex ASE350) using dichloromethane (DCM):methanol (MeOH) 9:1 for six cycles of five minutes (static  
110 time), 100  $^{\circ}\text{C}$ , and 2,000 psi. After extraction, we spiked the total lipid extract (TLE) with 1000 ng of 3-methyl-heneicosane  
111 (CAS#: 6418-47-9, Sigma-Aldrich), 20 ng of p-terphenyl (CAS#: 92-94-4, TCI), and 50 ng of pregnanol (5 $\beta$ -Pregnan-3 $\alpha$ -ol,  
112 CAS#: 4352-07-2, Steraloids) as internal standards for the quantification of *n*-alkanes, PAHs, and sterols, respectively. We  
113 concentrated the TLE under a gentle flow of nitrogen and then mixed it with HCl-activated copper shots to remove elemental  
114 sulphur as copper sulphide precipitates. We then filtered the samples through a  $\text{NaSO}_4$ -packed Pasteur column to remove any  
115 residual water and copper sulphide and concentrated them under  $\text{N}_2$ . We subsequently separated the TLE into six  
116 chromatographic fractions using a Pasteur pipette packed with silica gel (60–200  $\mu\text{m}$  - 60 A) and solvents of increasing polarity.  
117 We calculated the column’s dead volume (DV) with *n*-hexane, and then eluted samples with 1.5 DV of *n*-hexane (F1), 2 DV  
118 of *n*-hexane:DCM 4:1 (F2), 1.5 DV of DCM (F3), 2 DV of DCM:acetonitrile (F4), 1.5 DV of acetonitrile (F5), and 3 DV of  
119 MeOH (F6). We derivatised fraction F4, containing the sterols/stanols, using TMS-BSTFA (Supelco) and pyridine (50:50) at  
120 70  $^{\circ}\text{C}$  for 15 minutes, then dried under  $\text{N}_2$  and redissolved it in *n*-Hexane. We added 1 ng of p-terphenyl  $\text{D}_{14}$  (CAS: 1718-51-  
121 0, Sigma-Aldrich) and 50 ng of 5 $\alpha$ -cholestane (CAS: 481-21-0, Sigma-Aldrich) to fractions F2 (PAHs) and F4 (sterols),  
122 respectively, as injection standards to check the recovery and quantification consistency of analyses.



123 We analysed the *n*-alkanes, PAHs, and sterols using a Thermo Scientific Trace 1310 gas chromatograph (GC) equipped with  
124 a PTV inlet and a Restek glass liner interphase to a TSQ8000-Evo triple quadrupole mass spectrometer (MS). We used a 60  
125 m DB1 column (DB-1MS, 0.25 mm, 0.25  $\mu\text{m}$  film thickness, Agilent, USA) to separate *n*-alkanes and a DB-5 column (DB-  
126 5MS, 0.25 mm, 0.25  $\mu\text{m}$  film thickness, Agilent, USA) for PAHs and sterols, and He ( $1.2 \text{ ml min}^{-1}$ ) as a carrier gas. For *n*-  
127 alkane analysis, we injected samples in splitless mode at  $65 \text{ }^\circ\text{C}$  and the PTV was ramped to  $400 \text{ }^\circ\text{C}$  at  $3 \text{ }^\circ\text{C s}^{-1}$  and held for 5  
128 min. The GC oven temperature was programmed from  $60 \text{ }^\circ\text{C}$  to  $220 \text{ }^\circ\text{C}$  ( $25 \text{ }^\circ\text{C min}^{-1}$ ) and then to  $315 \text{ }^\circ\text{C}$  ( $2.5 \text{ }^\circ\text{C min}^{-1}$ , held  
129 13 min). *n*-Alkanes were analysed in full scan ( $50\text{--}600 \text{ m/z}$ ) using the following MS conditions:  $300 \text{ }^\circ\text{C}$  EI source at 70 eV  
130 electron energy, 50  $\mu\text{A}$  emission current, and 15 V electron lens voltage, with a transfer line at  $315 \text{ }^\circ\text{C}$ . For PAH analysis, all  
131 samples were injected in splitless mode at  $45 \text{ }^\circ\text{C}$  and the PTV was ramped to  $400 \text{ }^\circ\text{C}$  at  $11.6 \text{ }^\circ\text{C s}^{-1}$  and held for 2 min. The GC  
132 oven temperature was programmed from  $60 \text{ }^\circ\text{C}$  (held 1 min), to  $150 \text{ }^\circ\text{C}$  ( $40 \text{ }^\circ\text{C min}^{-1}$ ), to  $320 \text{ }^\circ\text{C}$  ( $3 \text{ }^\circ\text{C min}^{-1}$ , held 15 min). MS  
133 conditions were as follows:  $250 \text{ }^\circ\text{C}$  EI source at 70 eV electron energy, 50  $\mu\text{A}$  emission current, and 15 V electron lens voltage,  
134 with a transfer line at  $320 \text{ }^\circ\text{C}$ . For sterol/stanol analysis, all samples were injected in splitless mode at  $90 \text{ }^\circ\text{C}$ , evaporated at  
135  $100 \text{ }^\circ\text{C}$  (0.1 min), and the PTV was ramped to  $400 \text{ }^\circ\text{C}$  at  $8 \text{ }^\circ\text{C s}^{-1}$  and held for 1 min. The GC oven temperature was programmed  
136 from  $80 \text{ }^\circ\text{C}$  (held 1 min), to  $200 \text{ }^\circ\text{C}$  ( $20 \text{ }^\circ\text{C min}^{-1}$ ), to  $320 \text{ }^\circ\text{C}$  ( $5 \text{ }^\circ\text{C min}^{-1}$ , held 20 min). MS conditions were as same as for *n*-  
137 alkanes. PAHs and sterols/stanols were analysed in selected reaction monitoring (SRM) using the collision energies and mass  
138 transitions reported in Table A1 and Table A2).

### 139 3.4 Analysis of air parcel back-trajectory patterns

140 To define the potential regional extent of airborne PAHs arriving to SVID's catchment area, we traced the back-trajectory of  
141 air parcels using HYSPLIT (hybrid single particle lagrangian integrated trajectory; Draxler et al., 1998; Stein et al., 2015).  
142 Using a modified version of an R script originally developed to trace precipitation patterns (Caves Rugenstein and  
143 Chamberlain, 2018), we analyse data from the NOAA Global Data Assimilation System (GDAS; resolution  $1^\circ$  by  $1^\circ$ ) at a six  
144 hours frequency tracing back trajectories for three days (72 h) and two weeks (336 h) during two years characterised by  
145 opposite North Atlantic Oscillation (NAO; Hurrell et al., 2003) configuration (2009-2010, NAO-; 2013-2014, NAO+; NOAA,  
146 2023). PAHs deposition, which is enhanced by low temperatures, occurs not only via precipitation but in dry conditions as  
147 well (Arellano et al., 2018; Feng et al., 2017; Golomb et al., 2001; Halsall et al., 2001). Thus, we present data for air parcel  
148 trajectories that did and did not produce precipitation within six hours from the endpoint (SVID), initialising the trajectories  
149 at four different altitudes: 1000, 1500, 2000 m asl (water vapour usually advects within an altitude of 2 km; Bershaw et al.,  
150 2012; Lechler and Galewsky, 2013; Wallace and Hobbs, 2006), and 150 m asl (SVID surface elevation).

## 151 4 Background on proxies

### 152 4.1 Polycyclic aromatic hydrocarbons (PAHs)

153 We use pyrogenic PAHs (pyroPAHs) as tracers for the frequency/intensity of fire episodes, and the PAH perylene as a biogenic  
154 PAH related to terrestrial organic matter input. PAHs are semi-volatile compounds that can be of pyrogenic, petrogenic, or  
155 biogenic origin (Kozak et al., 2017; Lima et al., 2005). Low molecular weight (LMW; see Table A1 for group definition)  
156 PAHs in their non-alkylated form (Page et al., 1999; Yunker et al., 2002) constitute the majority of the PAHs produced by the  
157 combustion of plant biomass, while the relative amount of high molecular weight (HMW) PAHs increases along with higher  
158 fire temperatures (McGrath et al., 2003). LMW PAHs tend to be airborne and show high aqueous solubility and higher  
159 volatility, whereas HMW PAHs are usually in a solid phase (associated to either soot or char), show lower volatility, and are  
160 likely sourced locally (Hoffmann and Wynder, 1977; Junk and Ford, 1980; Karp et al., 2020; Lammel et al., 2009; Lima et al.,  
161 2005; Purushothama et al., 1998). Thus, low contributions of HMW PAHs in environmental samples are often considered  
162 indicative of either low temperature fires (e.g., Denis et al., 2012) or a distal source, while high relative amounts generally



163 point toward a more local signal. Finally, perylene is a 5-hexa-ring PAH often detected in aquatic sediments and considered  
164 to be mostly of in situ biogenic origin, probably from precursor compounds present in saprophagous and mycorrhizal fungi  
165 (e.g., Aizenshtat, 1973; Jiang et al., 2000; Slater et al., 2013; Wang and Huang, 2021), and thus likely linked to higher organic  
166 matter content and terrigenous input (Guo and Liao, 2020; Hanke et al., 2019).

#### 167 **4.2 Sterols/stanols as markers of plant sources and animal digestion**

168 Stanols are saturated isomers of sterols (e.g., Patterson, 1971). When the bacterially mediated reduction of sterol double bonds  
169 occurs in an open environment (e.g., soil), it leads almost exclusively to the production of 5 $\alpha$  stanol isomers. When the  
170 reduction of sterols occurs in the animal's digestive track, their enteric bacterial flora maximises the production of 5 $\beta$  stanols  
171 (Hatcher and McGillivray, 1979; Murtaugh and Bunch, 1967). Humans (and partially other omnivores and carnivores)  
172 maximise the production of coprostanol (5 $\beta$ -cholestan-3 $\beta$ -ol) through the saturation of animal derived cholesterol (5-en-  
173 cholest-3 $\beta$ -ol). Ruminants such as sheep and cattle, on the other hand, maximise the production of 5 $\beta$ -stigmastanol and 5 $\beta$ -  
174 campestanol (Leeming et al., 1996, 1994) from plant derived sterols like stigmasterol, sitosterol, and campesterol (e.g., Goad,  
175 1977; Goad and Goodwin, 1966; Pancost et al., 2002). Higher/lower ratios of coprostanol and its derived epimer epi-  
176 coprostanol (5 $\beta$ -cholestan-3 $\alpha$ -ol; McCalley et al., 1981; Quirk et al., 1980; Wardroper et al., 1978) to 5 $\beta$ -stigmastanol or 5 $\beta$ -  
177 campestanol are considered to be a proxy for higher/lower faecal input from human sources relative to ruminant sources, and  
178 have been widely applied to samples from modern/ancient sewage material and manured soil (e.g., Birk et al., 2012; Bull et  
179 al., 2001, 2002; Cordeiro et al., 2008; Evershed et al., 1997; He et al., 2018; Lerch et al., 2021; Simpson et al., 1999; Tyagi et  
180 al., 2009).

#### 181 **4.3 *n*-Alkanes**

182 Plants synthesise *n*-alkanes and other *n*-alkyl lipids as part of their waxy coating with a characteristic strong odd-over-even  
183 chain length predominance (Eglinton and Hamilton, 1967), which is summarised by their higher carbon preference index (CPI;  
184 Bray and Evans, 1961; Marzi et al., 1993). In contrast, lower CPI values are usually indicative of petrogenic, algal, or bacterial  
185 sources (Grimalt and Albaigés, 1987; Han and Calvin, 1969). Aquatic sources such as macrophytes and mosses (e.g.,  
186 *Sphagnum*) maximise their leaf wax *n*-alkane production at mid-length homologues (C<sub>21–25</sub>), while terrestrial plants (e.g.,  
187 grasses, sedges, trees, shrubs) are generally skewed toward longer homologues (C<sub>27–31</sub>), allowing for use of source  
188 discriminating ratios and indices (e.g., aquatic plant index, Ficken et al., 2000; average chain length, Gagosian and Peltzer,  
189 1986).

#### 190 **4.4 Bulk geochemistry proxies**

191 Aquatic and terrestrial catchment productivity, flux of inorganic sediments, and organic matter preservation are the main  
192 factors determining the level of total organic carbon content in lacustrine sediments (Meyers and Ishiwatari, 1993). The molar  
193 carbon to nitrogen ratio (C/N) in plant tissue varies between aquatic plants and phytoplankton (<10) and terrestrial plants and  
194 bryophytes (>10; Meyers, 1994). Thus, increases in C/N are usually interpreted as an increased catchment erosion and input  
195 of terrestrial organic matter and/or as a relative decrease of aquatic plant productivity (Fernández-Martínez et al., 2021;  
196 Kaushal and Binford, 1999; Meyers, 1997; Meyers and Teranes, 2001; Rieger et al., 1979). Shifts in the abundance of diatom  
197 derived biogenic silica (BSi) can trace lake productivity (Colman et al., 1995; Conley, 1988; Conley and Schelske, 2002). The  
198 conservation potential of diatom frustules is strongly related to sedimentation rate, with higher rates leading to better  
199 preservation. When sedimentation rates are considered relatively constant, shifts in BSi can reflect qualitative changes in  
200 spring/summer temperature in high-latitude lakes, such as Iceland (Geirsdóttir et al., 2009a; McKay et al., 2008). The stable  
201 isotopic composition of carbon ( $\delta^{13}\text{C}$ ) can trace shifts in the relative contribution of organic matter sources, with terrestrial  
202 plants (but also bryophytes) and associated soils showing more  $^{13}\text{C}$ -depleted values (ca -32‰ to -25‰), aquatic plants





203 exhibiting more  $^{13}\text{C}$ -enriched values (ca -20‰ to -10‰), and freshwater algae and phytoplankton showing a wider isotopic  
204 range (Meyers, 1994; Prokopenko et al., 1993; Rundel et al., 1979; Smith and Epstein, 1971; Geirsdóttir et al., 2020 and refs  
205 therein). The physical mixing or stratification of a lake water column can also influence the carbon isotopic signature of aquatic  
206 sources (Hernández et al., 2011).

## 207 5 Results

### 208 5.1 Age model

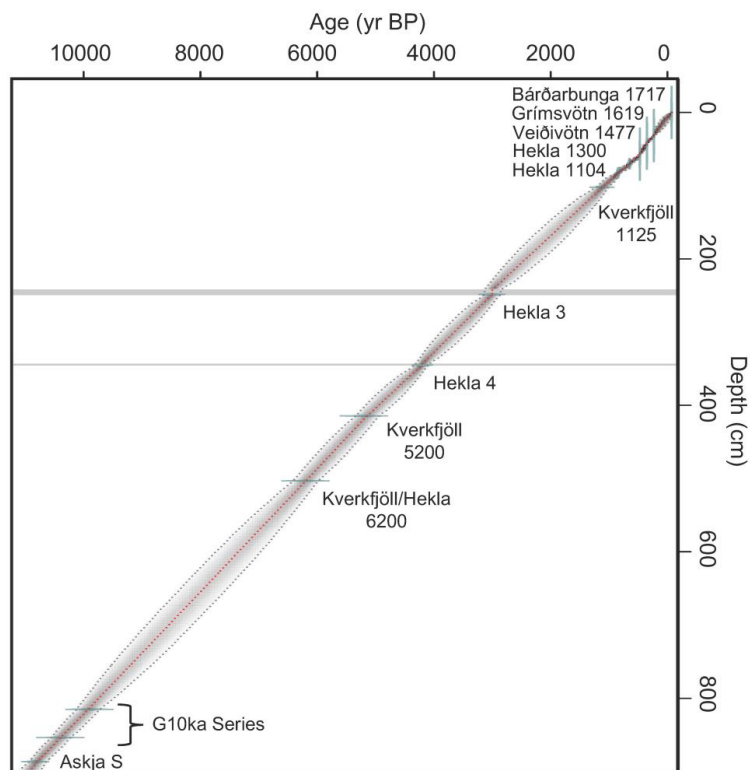
209 Based on major oxide composition and stratigraphical information, we identified 13 marker tephra layers of known age (Table  
210 1). Our Bayesian tephra age model shows nearly constant sediment accumulation rates throughout the Holocene (Fig. 2).  
211 There is increased uncertainty in age control between the G10ka tephra series and Kverkfjöll/Hekla 6200 due to fewer marker  
212 tephra layers being present. However, the Late Holocene, particularly during the historical period of settlement, features  
213 numerous tephra layers that result in substantially lower age estimate uncertainty.

214

215 **Table 1: Marker tephra layers of known age identified in 20-SVID-02 and used to develop the age model.**

Composite depth (cm)	Tephra layer ID	Layer age (a BP)	Reference
31.5	Bárðarbunga-Veiðivötn 1717	$233 \pm 2$	Thorarinsson (1974)
42.0	Grímsvötn 1619?	$352 \pm 2$	Thorarinsson (1974)
56.0 – 57.0	Veiðivötn 1477	$473 \pm 2$	Larsen et al. (2002)
70.0	Hekla 1300	$650 \pm 10$	Thorarinsson (1967)
82.5	Hekla 1104	$846 \pm 10$	Thorarinsson (1967)
102.2	Kverkfjöll	$1125 \pm 50$	Óladóttir et al. (2011)
242.5 – 248.5	Hekla 3	$3010 \pm 54$	Dugmore et al. (1995)
344.0 – 345.0	Hekla 4	$4200 \pm 42$	Dugmore et al. (1995)
414.0 – 414.5	Kverkfjöll	$5200 \pm 100$	Óladóttir et al. (2011)
503.2	Kverkfjöll and Hekla	$6200 \pm 100$	Óladóttir et al. (2011)
815.0	G10ka Series (top)	9900	Óladóttir et al. (2020)
853.5	G10ka Series (bottom)	10400	Óladóttir et al. (2020)
886.5	Askja S	$10830 \pm 57$	Bronk Ramsey et al. (2015)

216



217

218 **Figure 2: Stóra Viðarvatn age model generated in Bacon (Blaauw and Christeny, 2011). Green horizontal lines denote the age and**  
 219 **uncertainty of marker tephra layers, red line reflects mean values of model iterations, the grey lines denote the 95% confidence**  
 220 **envelope, and darker shading reflects more likely ages. Gray vertical bars mark the ‘slumps’ used for the Hekla 3 and Hekla 4**  
 221 **tephra layers.**

222

223 To facilitate the interpretation of downcore records, we present and discuss data (1) divided into nine time intervals (I–IX;  
 224 Table 2) representing the most distinguishable periods of variability with respect to background values, and (2) separately for  
 225 the sections preceding and following the G10ka tephra series (Óladóttir et al., 2020).

226

227 **Table 2: Age intervals (approximate) and descriptions of the nine subdivisions of the 20-SVID-02 record used in this study.**

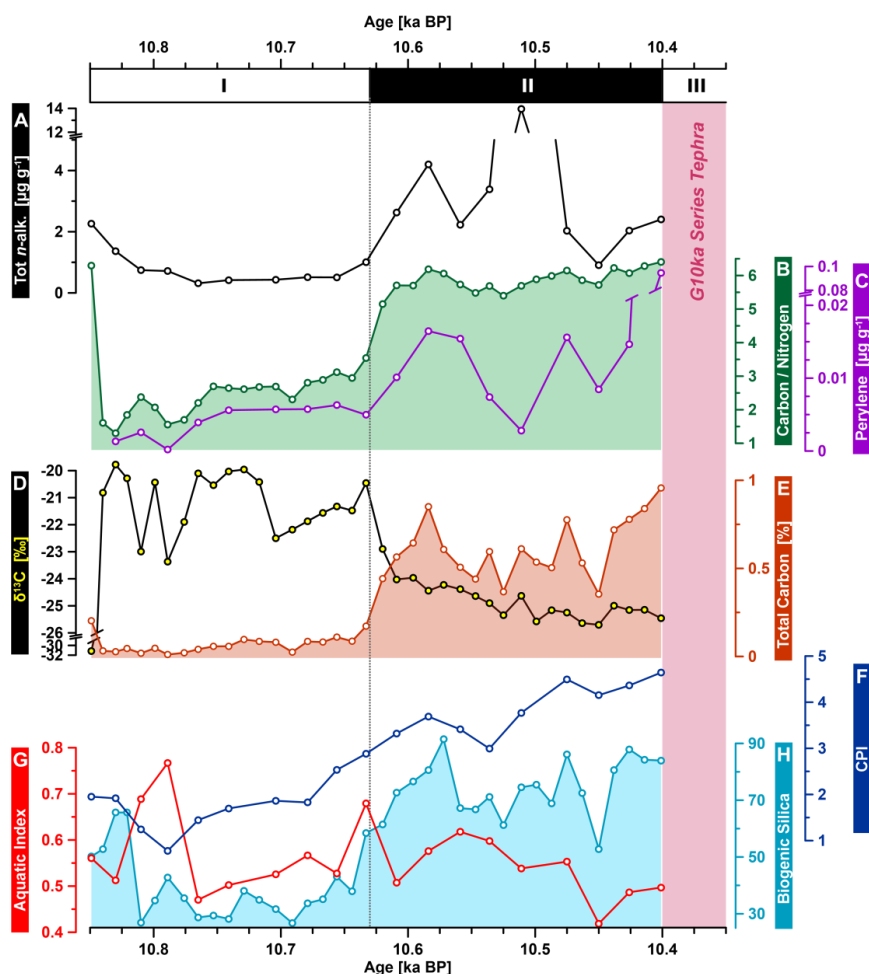
Interval	Age (ka BP)	Description
I	10.85–10.63	Potential Preboreal cooling
II	10.63–10.40	Pre-Boreal warming
III	10.4–9.9	G10 ka tephra series
IV	9.9–8.8	Early Holocene warming (rebound after G10 ka event)
V	8.8–7.5	Early Holocene instability (8.2 ka event?)
VI	7.5–3.0	Middle Holocene plateau and trend inversion
VII	3.0–1.3	Late Holocene cooling
VIII	1.3–0.25	Medieval period and Little Ice Age
IX	0.25–present	End of LIA and contemporary warming

228



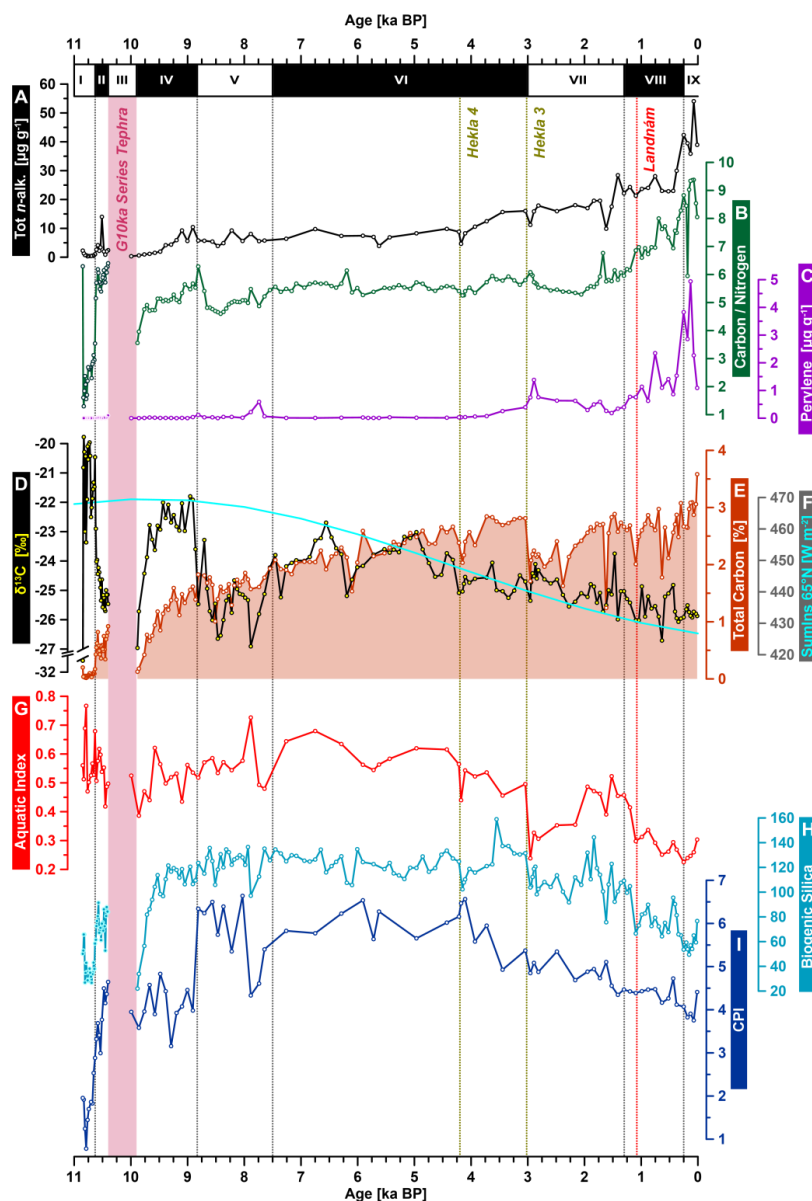
## 229 5.2 Bulk geochemistry

230 The C/N ratio (Figs. 3-4B) ranged from ~1 to ~9.5, showing lowest values at the beginning of the record (I). At ca 10.63 ka  
 231 BP, C/N increased sharply and reached mid-range values (5-6), remaining relatively stable throughout most of the remaining  
 232 Holocene (IV–VI), except for two drops, after the G10ka Series tephra and between 8.8 and 7.75 ka BP (V). In the last 2 kyr,  
 233 C/N values steadily increased, leading to the highest values in the most recent portion of the record. The two periods with  
 234 decreased C/N values, as well as the initial increase (I to II), generally paralleled the behaviour of the total carbon (Figs. 3-  
 235 4E), biogenic silica (Figs. 3-4H), and  $\delta^{13}\text{C}$  (Figs. 3-4D) records. TC increased steadily throughout the Holocene from ~0%  
 236 while BSi rapidly increased at the beginning of the record (30 to 90) to then stabilise at 110–120 for more than 5 kyr (V–VI).  
 237 Both records peaked at ca 3.5 ka BP (2.8%, TC; ~160, BSi max) and temporarily dropped between ca 3 and 2.25 ka BP.  
 238 Subsequently, TC increased to its maximum value (3.6%, modern) while BSi decreased in a stepwise manner, reaching its  
 239 lowest value of the last 10 kyr (~50) at ca 0.2 ka BP. The  $\delta^{13}\text{C}$  record showed the most  $^{13}\text{C}$ -enriched values (-20‰) in the  
 240 oldest interval (I); it then decreased (to -26‰, modern) steadily throughout the Holocene, except for two major drops to its  
 241 most depleted values (ca -27‰) during periods II and V.



242

243 **Figure 3: Erosional and primary productivity proxies from the pre-G10ka Series tephra interval (pink vertical band) of 20-SVID-**  
 244 **02 core; all concentrations are on g of dry samples. (A, black) sum of C<sub>19-35</sub> n-alkanes concentration aquatic plant index derived**  
 245 **from n-alkanes; (B, green) carbon to nitrogen ratio; (C, purple) perylene concentration; (D, black-yellow) stable isotopic composition**  
 246 **of total carbon; (E, brick red) percentage of total carbon; (F, dark blue) n-alkanes carbon preference index (CPI<sub>19-31</sub>); (G, red)**  
 247 **aquatic plant index derived from n-alkanes; (H, light blue) biogenic silica.**



248

249 **Figure 4:** Erosional and primary productivity proxies of 20-SVID-02 core. (A, black) sum of  $C_{19-35}$  *n*-alkanes concentration aquatic  
 250 plant index derived from *n*-alkanes; (B, green) carbon to nitrogen ratio; (C, purple) perylene concentration; (D, black-yellow) stable  
 251 isotopic composition of carbon; (E, brick red) percentage of total carbon; (F, cyan) northern hemisphere summer insolation at 65°  
 252 N (Berger and Loutre, 1999); (G, red) aquatic plant index derived from *n*-alkanes; (H, light blue) biogenic silica; (I, dark blue)  
 253 carbon preference index (CPI<sub>19-31</sub>). Red dotted line marks the conventional age (870 CE) of the settlement of Iceland (Landnám).  
 254 Black vertical dashed lines mark the subdivision of the 20-SVID-02 record into nine intervals (Table 1).

### 255 5.3 *n*-Alkanes

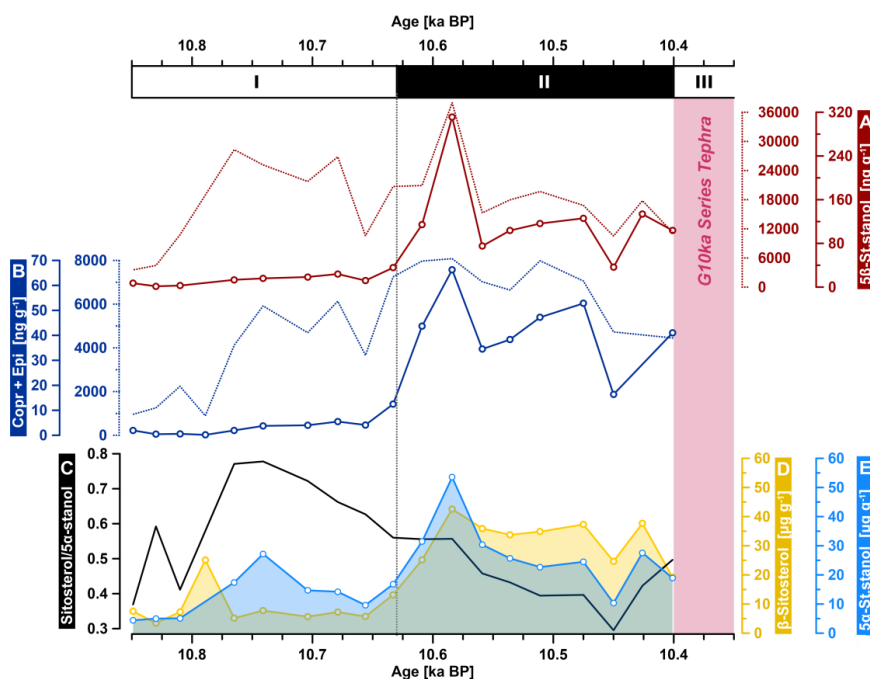
256 We detected *n*-alkane homologues from  $C_{19}$  to  $C_{33-35}$  (Fig. A3) in most samples, with a total sum that ranged from 0.3 to 50  
 257  $\mu\text{g g}^{-1}$  (700–4000  $\mu\text{g g}^{-1}$  TC; Figs. 3-4A). The 10.8 to 4.2 ka BP interval showed relatively low and stable values ( $\sim 5 \mu\text{g g}^{-1}$ );  
 258 concentrations roughly doubled from 4 to 1.5 ka and then again after 0.5 ka BP, reaching its maximum value at the end of the  
 259 record. The CPI showed a stable odd-over-even predominance (3 to 6.5) through the whole record, except for low values (1 to  
 260 3) seen in the interval preceding the G10ka Series tephra (Figs. 3F-4I). The most abundant homologues were  $C_{23-27}$  (45%) in



261 the 10.8 to 3 ka BP interval and  $C_{29-31}$  (40%) in the last 3 kyr. This regime change was highlighted by a shift in  $P_{aq}$  from  
262 relatively high values (up to 0.8; avg. 0.6) through the early-mid Holocene to lower values (down to 0.2; avg. 0.3) after 3 ka  
263 BP (Fig. 4G).

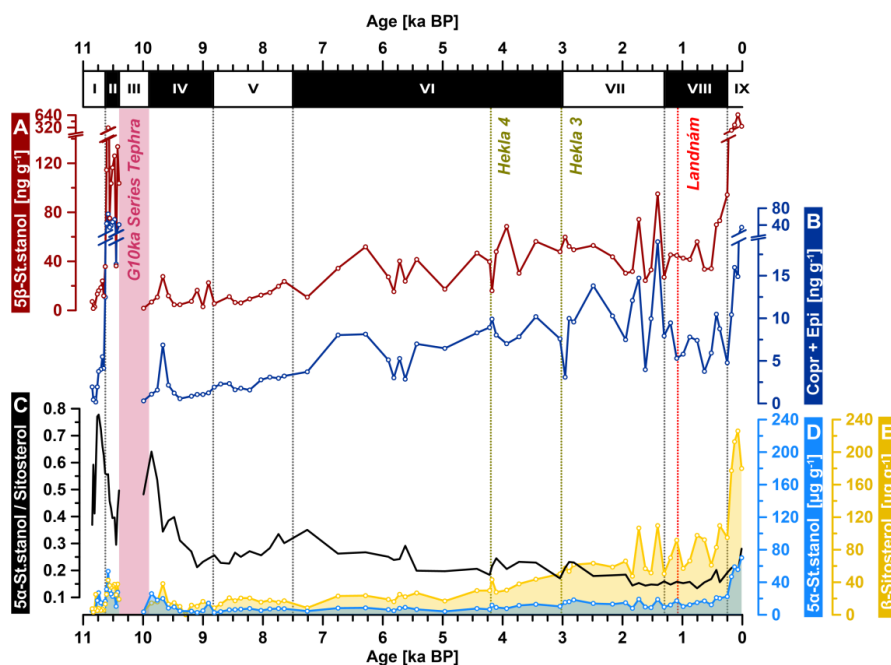
#### 264 5.4 Faecal sterol/stanols

265 We detected the three main faecal stanols: the plant derived  $5\beta$ -stigmastanol was ~5–10 times more abundant (up to 3-500 ng  
266  $g^{-1}$ ; Figs. 5-6A) than coprostanol + epi-coprostanol (10-30 ng  $g^{-1}$ ; Figs. 5-6B). The oldest interval (I) showed the lowest  
267 concentrations for all three stanols, while the following interval (II) displayed high (highest for coprostanol and epi-  
268 coprostanol) concentrations. All three stanols showed low and stable concentrations between ~9.5 and 7.5 ka BP, gradually  
269 increased from ~7.5 ka BP before reaching a relative maximum around 1.5 ka BP (VII), dropping again during interval VIII,  
270 and peaking during the last 200 to 300 years (IX). Parent sterols ( $\beta$ -sitosterol,  $\beta$ -stigmasterol, except cholesterol) and the  $\alpha$ -  
271 stanol isomers, follow patterns similar to the  $\beta$ -stanols throughout the Holocene, but with 10 to 100 times higher concentrations  
272 (Fig. A2).



273

274 **Figure 5:** Sterols/stanols from the pre-G10ka Series tephra interval (pink vertical band) of 20-SVID-02 core. (A, red)  $5\beta$ -stigmastanol  
275 and (B, dark blue) sum of coprostanol and epi-coprostanol concentration on g of dry sample (full line) and on g of TC (dotted line);  
276 (C, black)  $\beta$ -sitosterol to  $5\alpha$ -stigmastanol ratio; (D, yellow)  $\beta$ -sitosterol concentration; (E, light blue)  $5\alpha$ -stigmastanol concentration.

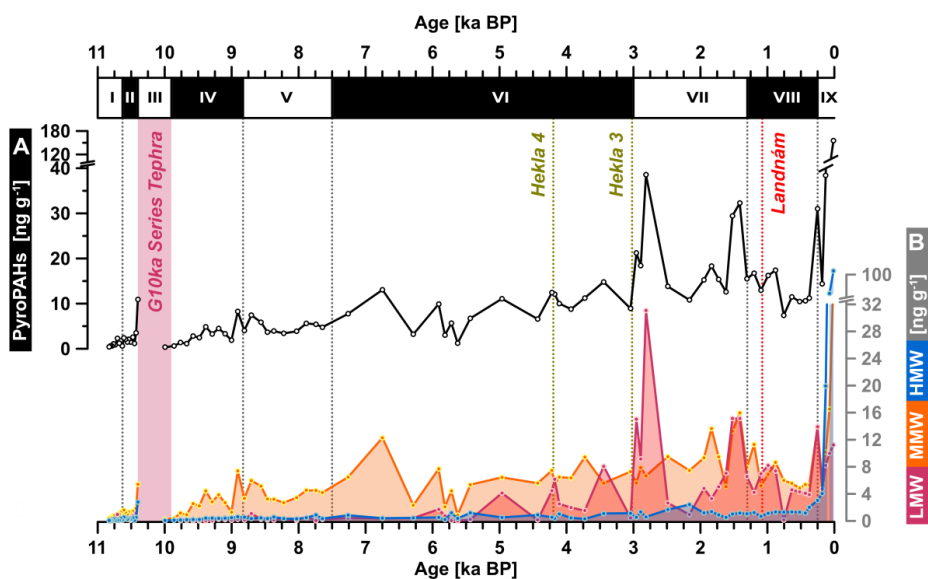


277

278 **Figure 6:** Sterols/stanols of the 20-SVID-02 core. (A, red)  $5\beta$ -stigmastanol and (B, dark blue) sum of coprostanol and epi-coprostanol  
279 concentration on g of dry sample (full line) and on g of TC (dotted line); (C, black)  $\beta$ -sitosterol to  $5\alpha$ -stigmastanol ratio; (D, yellow)  
280  $\beta$ -sitosterol concentration; (E, light blue)  $5\alpha$ -stigmastanol concentration. Red dotted line marks the conventional age (870 CE) of the  
281 settlement of Iceland (Landnám). Black vertical dashed lines mark an arbitrary subdivision of 20-SVID-02 record into nine intervals  
282 (Table 1).

### 283 5.5 Polycyclic aromatic hydrocarbons (PAHs)

284 PAHs were present in all samples and generally in higher concentrations in more recent compared to older samples (Fig. A1).  
285 Perylene (Figs. 3-4C), which accounts for more than 97% of detected PAHs, maintains low concentrations ( $0\text{--}20\text{ ng g}^{-1}$ ) from  
286 10.5 to 4-3 ka BP. A first increase to  $0.5\text{--}1.5\text{ }\mu\text{g g}^{-1}$  occurred between 3.5 and 2.8 ka BP, followed by a decrease loosely coeval  
287 to the decrease in TC and BSi (VII). After ca 1.5 ka BP, perylene increases to a maximum value ( $\sim 6\text{ }\mu\text{g g}^{-1}$ , ca 0.15 ka BP),  
288 which generally matches the pattern of TC. The second most abundant compound was phenanthrene ( $0.01\text{--}31.1\text{ ng g}^{-1}$ ),  
289 followed by pyrene ( $0.1\text{--}11.5\text{ ng g}^{-1}$ ) and fluoranthene ( $0.01\text{--}17.6\text{ ng g}^{-1}$ ). The least abundant PAHs were naphthalene,  
290 acenaphthylene and acenaphthene. However, since the detection of these three low molecular weight compounds could have  
291 been influenced by evaporation losses during sample preparation, their reported concentrations are likely to be underestimated.  
292 Given the overwhelming dominance of perylene and its likely biogenic rather than pyrogenic origin, we removed it from total  
293 PAHs abundance calculations to provide a record with features that were not apparent in perylene's trend. In terms of total  
294 pyroPAHs abundance, we observe five distinguishable intervals (Fig. 7A). First, a 3 kyr-long interval ( $\sim 80$  years average  
295 temporal resolution) starting at ca 10.5 ka BP displays a relatively stable low concentrations ( $< 5\text{ ng g}^{-1}$ ,  $\text{SD } \sigma = 2.3$ ). The only  
296 exception is a point taken within the G10ka Series tephra (up to  $10\text{ ng g}^{-1}$ ) at ca 10 ka BP. Second, from  $\sim 7.5$  to 2.9 ka BP  
297 ( $\sim 320$  years average temporal resolution), the total PAHs concentration increases from  $\sim 5$  to  $10\text{ ng g}^{-1}$ , although with enhanced  
298 variability ( $\sigma = 3.7$ ). Third, led by the increase of low molecular weight PAHs (LMW, Fig. 7B), during the 2.9 to 0.7 ka BP  
299 interval, values fluctuate ( $\sigma = 7.5$ ) between  $\sim 10$  and  $20\text{ ng g}^{-1}$ , with two major peaks reaching  $45$  and  $35\text{ ng g}^{-1}$  at  $\sim 2.7$  to 2.3  
300 ka BP and 1.5 to 1.3 ka BP, respectively. Fourth, between 0.7 and 0.3 ka BP there is a relatively brief although clear drop ( $\sim 10$   
301  $\text{ng g}^{-1}$ ,  $\sigma = 1.5$ ), led by both LMW and MMW PAHs. In the last 250 years we observe a sharp, 10-fold increase in PAHs  
302 concentration leading to the highest recorded values ( $\sim 200\text{ ng g}^{-1}$ ). When normalised for TC (Fig. A1), the absolute values  
303 increase 10 to 100-fold, but the patterns do not substantially change.



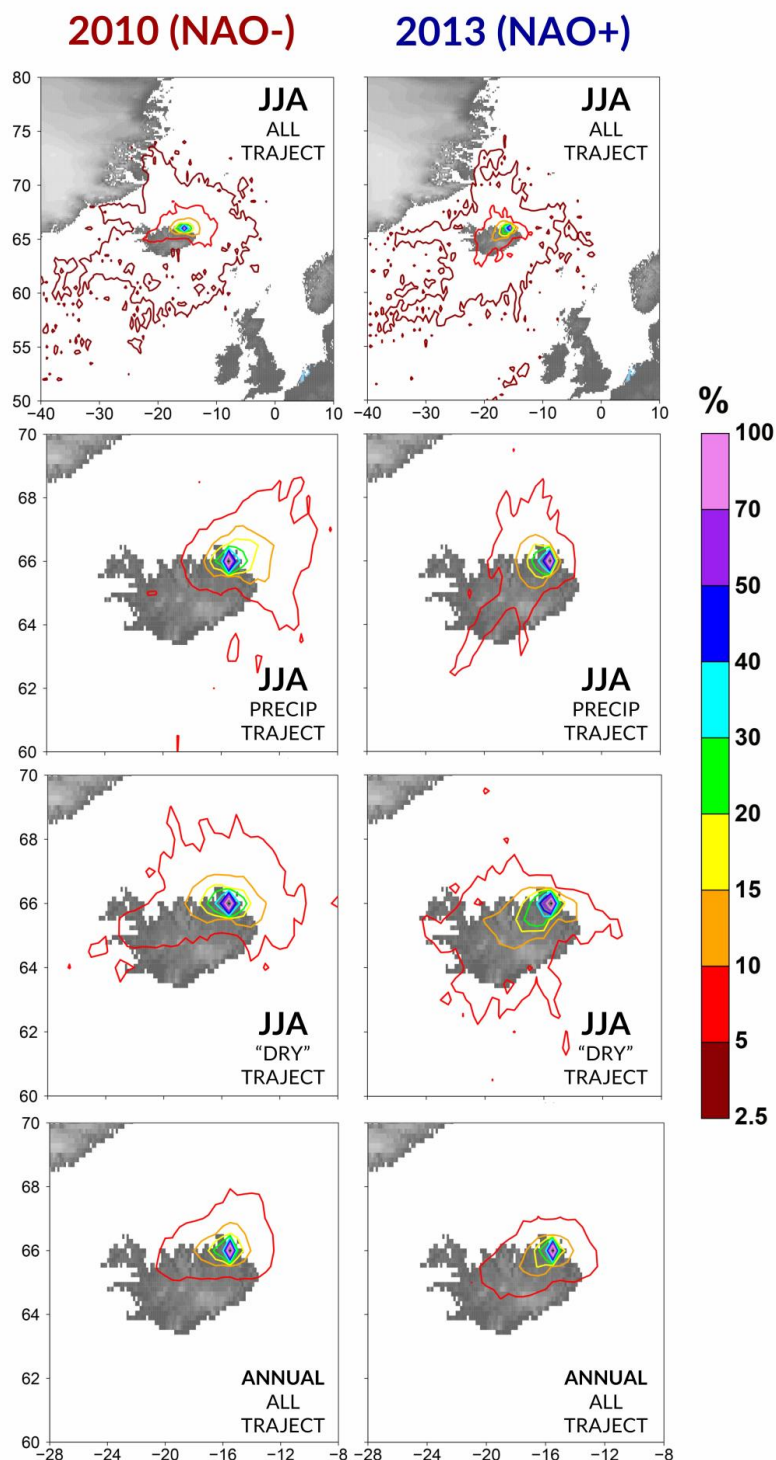
304

305 **Figure 7:** PAHs record of the 20-SVID-02 core. (A, black) sum of pyrogenic PAHs concentrations; (B, fuchsia) low, (orange) medium,  
306 and (blue) high molecular weight pyrogenic PAHs concentration. Red dotted line marks the conventional age (870 CE) of the  
307 settlement of Iceland (Landnám). Vertical pink band marks the G10ka Series Tephra. Black vertical dashed lines mark an arbitrary  
308 subdivision of 20-SVID-02 record into nine intervals (Table 1).

## 309 5.6 HYSPLIT

310 We calculated a total of 11,392 air trajectories, which we split by year, season, dry (i.e., not associated with precipitation), or  
311 precipitation bearing trajectories (Fig. A4). Most trajectories, even for two weeks intervals, show air parcels originating mostly  
312 from Iceland and surrounding areas of the North Atlantic, regardless of season or NAO configuration, while the contribution  
313 from nearby terrestrial regions (potential PAHs sources) such as Greenland, British Isles, or Scandinavia is negligible. As the  
314 marine environment is not conducive to combustion nor redeposition of particulates, this implies a dominantly Icelandic signal  
315 for PAH production.

316 Since wildfires are concentrated in the relatively dryer, snow-free summer season (McCarty et al., 2021), we focus particularly  
317 on the JJA air trajectory data (Fig. 8). These results show that: (1) 95% of back-trajectories originate from Iceland and its  
318 nearby waters; (2) 90% of back-trajectories originate within 100–150 km radius from SVID; (3) dry trajectories more likely  
319 originate inland relative to precipitation carrying trajectories; (4) 95% of trajectories from a NAO- year tend to be confined to  
320 northern Iceland while during a NAO+ year trajectories more commonly originate from inland; (5) these patterns are consistent  
321 even when scaled from three days to two weeks intervals (Fig. A4).



322

323 **Figure 8:** HYSPLIT back trajectories of air parcels for 2010 (NAO-) and 2013 (NAO+), annual and summer (JJA). Trajectories are  
 324 calculated on a two-weeks (336 h) interval at a 6-hour frequency; “precip” indicates trajectories that produced precipitation within  
 325 6 h from the SVID endpoint, while “dry” trajectories did not. Contour colours indicate the frequency at which air parcels part of a  
 326 trajectory travel above a certain area.





## 327 6 Discussion

### 328 6.1 Primary aquatic production vs erosion/terrestrial input

329 In Icelandic lacustrine environments,  $\delta^{13}\text{C}$  and C/N are generally considered proxies for the relative contribution of terrestrial  
330 vs aquatic organic matter and shifts in primary productivity, as total carbon is virtually solely of organic origin (e.g., Geirsdóttir  
331 et al., 2009a). In SVID, the similarity of the C/N record to the perylene curve reinforces its significance as a proxy for  
332 terrigenous input.

#### 333 6.1.1 11-7.5 ka BP: Postglacial warming

334 Deglaciation in the NE of Iceland set in between 15 and 13 ka BP and proceeded in a stepwise fashion, with two main glacier  
335 re-advances at ca 12.7 (Younger Dryas) and 10.9 ka BP (Preboreal; Geirsdóttir et al., 2009b; Norðdahl and Pétursson, 2005).  
336 Our record captures sediment below the Askja S tephra layer ( $10.83 \pm 0.57$  ka BP, Bronk Ramsey et al., 2015), showing ice-  
337 free conditions and the start of organic sedimentation by 10.85 ka BP at SVID's location. Except for the oldest sample, high  
338  $\delta^{13}\text{C}$  and low TC values indicate a primarily aquatic source of carbon during the oldest interval (I) (Fig. 3). This suggests an  
339 absence of substantial terrestrial vegetation, consistent with a postglacial landscape and possibly a cooler climate associated  
340 with the Preboreal period.

341 TC, BSi, and C/N increase suddenly at ca 10.65 ka BP, maintaining higher values for two-three centuries (vice versa for  $\delta^{13}\text{C}$ ),  
342 indicating an enhanced terrestrial input likely resulting from a retreating glacier, development of soil and vascular plants, and  
343 generally warming conditions (Fig. 3). After the G10ka Series tephra, all proxy values decrease, likely due to the destructive  
344 impact of substantial volcanic ash fallout on both terrestrial and aquatic vegetation and related water chemistry alteration (e.g.,  
345  $\delta^{13}\text{C}$  dropping due to acidification; Kilian et al., 2006) (Fig. 4). Following the volcanic event, all proxies increase at ca 9.75 ka  
346 BP, whereas terrestrial- relative to aquatic-sourced carbon temporarily increase (ca 8.7–7.5 ka BP). The observed decrease in  
347  $\delta^{13}\text{C}$  (and, partially, C/N) between 8.7 and 7.5 ka BP is identified in other Icelandic lake sediment records between 8.8 and 7.9  
348 ka BP (e.g., Eddudóttir et al., 2018; Geirsdóttir et al., 2013; Harning et al., 2018b; Larsen et al., 2012) and has been attributed  
349 to the likely impact of meltwater pulses into the northern North Atlantic due to the retreating Laurentide ice sheet and/or local  
350 effusive volcanic eruptions (Geirsdóttir et al., 2013; Larsen et al., 2012).

351 The total sum of *n*-alkanes ( $\text{C}_{19-35}$ ; Fig. 4A), which is heavily controlled by  $\text{C}_{29}$  and  $\text{C}_{31}$  (Fig. A3), increases throughout the  
352 Holocene similar to the pattern described by C/N and perylene as a result of an increased terrigenous input. As inferred by  
353 high CPI values, most *n*-alkanes in SVID originate from plants (terrestrial and possibly also aquatic) through the Holocene  
354 record (Fig. 4I). The relatively low CPI values in the oldest interval (I) indicate a negligible contribution from plant sources  
355 (relative to phytoplankton) to the carbon pool, which is consistent with a still cold, relatively barren, deglacial environment.

356 The CPI curve shows a similar but opposite pattern to the  $\delta^{13}\text{C}$  record until ca 8 ka BP, reinforcing  $\delta^{13}\text{C}$  as a proxy mostly  
357 controlled by terrigenous input (*n*-alkanes from aquatics show lower CPI values than terrestrial plants; e.g., Bray and Evans,  
358 1961; Duan et al., 2014; Eglinton and Hamilton, 1967; Li et al., 2020). The reason for the change in the relationship between  
359 CPI and  $\delta^{13}\text{C}$  (which become positively correlated after 8 ka BP) is unclear. While it matches the timing of increasing  
360 temperatures (Axford et al., 2007; Fig. 10D) and *Betula* expansion in the region (Karlsdóttir et al., 2014; Fig. 10E), its  
361 interpretation is complicated by the fact that CPI can also be influenced by factors such as changes in mean annual precipitation,  
362 seasonality, plant community, and algal productivity (Li et al., 2020).

#### 363 6.1.2 7.5-4.2 ka BP: Mid-Holocene Plateau and trend inversion

364 Overall, all proxies suggest that the interval between ~7.5 and 4.2 ka BP, was characterised by relatively stable climatic  
365 conditions, generally warmer (Axford et al., 2007) and wetter (Moossen et al., 2015) than both the preceding and following  
366 periods. These conditions likely led to an enhanced primary productivity within the lake, as suggested by high values of BSi,



367  $P_{aq}$ , CPI, and pollen inferred vegetation communities (Eddudóttir et al., 2016; Karlsdóttir et al., 2014). In fact, modelled  
368 reconstructions of Icelandic vegetation cover throughout the Holocene show the highest values during this interval (Ólafsdóttir  
369 et al., 2001). In particular, partly due to the retreat/disappearance of most glaciers, between 50% and 60% of Iceland was likely  
370 covered in vegetation, of which a quarter was birch forest, throughout the mid-Holocene, with two peaks, one at the Holocene  
371 Thermal Maximum (8–7 ka BP) and one at ~3.5 ka BP (Ólafsdóttir et al., 2001). The warm and moist climate, paired with the  
372 expansion of vegetation, may have stabilised the local environment, reducing erosion. Such stability is consistent with the low  
373 C/N, Perylene, and *n*-alkanes values throughout this interval.

374 Though this four thousand year period is broadly categorised by stability, a more detailed view reveals important inflection  
375 points in the long term trends of many proxies. For example, while some proxies keep increasing (e.g., TC, and summer  
376 temperature, Axford et al., 2007), some stop rising and remain relatively flat throughout this interval (e.g., C/N, Perylene),  
377 while others even invert their trends ( $\delta^{13}C$ ,  $P_{aq}$ , CPI). Another trend inversion occurred around 5 ka BP with the inception of  
378 neo-glaciation in Iceland when glaciers started to expand again (Geirsdóttir et al., 2019). This could be interpreted as a slow  
379 inertial response of the local environment to the decreasing NH summer insolation, likely reducing its resilience to short term  
380 events such as volcanic eruptions and NAO shifts, until some kind of threshold was finally reached around 4 ka BP (Geirsdóttir  
381 et al., 2013, 2019).

#### 382 **6.1.3 4.2 ka BP: Increased erosion in a cooling climate**

383 Our SVID proxy datasets generally agree with previous work using bulk geochemistry proxies in Icelandic lakes, which  
384 collectively point toward decreasing primary productivity and increasing landscape instability in response to declining  
385 Northern Hemisphere summer insolation (e.g., Geirsdóttir et al., 2013, 2019; Harning et al., 2018b, 2020; Larsen et al., 2012).  
386 The decreasing trend in  $\delta^{13}C$  is generally anticorrelated with the TC curve, indicating that TC is increasingly controlled by  
387 terrestrial input. BSi, TC, and C/N values drop or invert their trend after ca 4 ka BP, consistent with a general decrease in  
388 productivity. This is possibly related to a combination of decreasing moisture and/or summer temperatures (Axford et al.,  
389 2007), and the effect of the Hekla 4 volcanic event, pushing the local environment beyond a threshold (Eddudóttir et al., 2017).  
390 Absolute amounts of *n*-alkanes also increase starting at 4 ka (Fig. 4A), led by an increase in *n*-C<sub>29</sub> (Fig. A3), typical of terrestrial  
391 plants. The ratio between the mid- and long-chain homologues (aquatic plant index or  $P_{aq}$ ; Ficken et al., 2000) is often  
392 interpreted as a proxy for a wetter/drier environment. However, this is likely an oversimplification as questions remain about  
393 the relationship between *n*-alkane chain length and vegetation source, particularly for aquatic plants which are often a minor  
394 component of the leaf wax pool in Arctic lakes (Dion-Kirschner et al., 2020; Hollister et al., 2022). Nevertheless, when coupled  
395 to the concentration data of *n*-alkanes (Fig. 4A; Fig. A3),  $P_{aq}$  can here be more safely interpreted as indicative of lower/higher  
396 terrigenous input. The SVID record (Fig. 4H; Sect. 4.3) shows higher  $P_{aq}$  values (mean 0.6) during the 10.8 to 4-3 ka BP  
397 interval, indicating an environment with significant aquatic plant production and likely limited erosion/in-wash. The record  
398 then switches abruptly to lower values (mean 0.3) at 3 ka BP, highlighting a shift toward greater in-wash of terrestrially derived  
399 material.

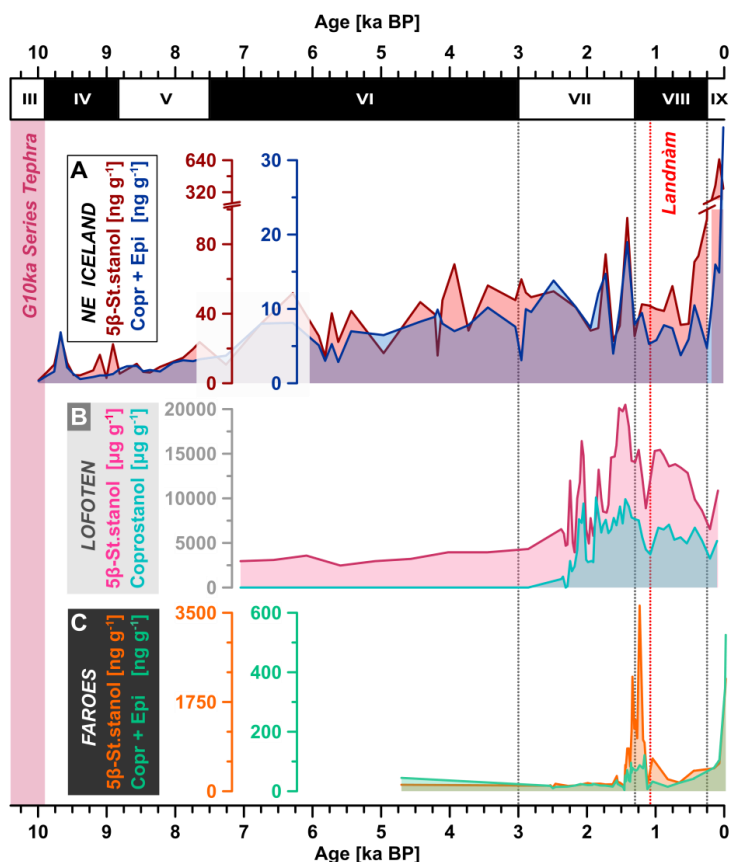
400 The massive Hekla 3 eruption (the most severe Hekla eruption of the Holocene; ~3,010 a BP; Larsen, 1977; Larsen and  
401 Eiríksson, 2008), was likely the cause, or at least the trigger, of this abrupt shift at 3 ka BP in most SVID proxy records,  
402 particularly the ones related to primary production and erosion (Larsen et al., 2011). In fact, the volcanic fallout likely killed  
403 terrestrial plants by burning, root suffocation, and reduced photosynthesis (e.g., Ifkirne et al., 2022; Mack, 1981; De Schutter  
404 et al., 2015), and had likely similar effects on aquatic flora as well, also through increased turbidity and acidity of lake waters  
405 (e.g., Ayris and Delmelle, 2012). The subsequent reduced coverage of terrestrial plants likely exposed the soil to increased  
406 erosion, resulting in more terrestrial in-wash (as reflected by a sudden perylene peak), skewed toward the inorganic components  
407 of soil (as reflected by a sudden drop in TC and *n*-alkanes lasting roughly a century). The increased terrestrial in-wash would  
408 have further reduced primary productivity within the lake, as suggested by the drop in BSi. At the same time, the short C/N



409 peak and the major drop in  $P_{aq}$  seem to indicate that the productivity and contribution of terrestrial plants remained higher than  
410 aquatic sources (Larsen et al., 2011). The post-3 ka trend is temporarily interrupted by what appears to be a partial rebound in  
411 primary productivity (BSi increases too) and diminished in-wash of terrestrial material until ca 1.5 ka BP, whereafter it  
412 continues to decline.

## 413 6.2 Is there geochemical evidence for human settlement in the SVID catchment area?

414 In paleoclimate studies, relative shifts to above natural background levels of  $\beta$ -stanols have been used as a proxy for human  
415 settlement, marking the appearance of humans and domesticated animals in specific areas of the world (Shillito et al., 2020;  
416 Sistiaga et al., 2014), often in lake catchments (Battistel et al., 2016; Callegaro et al., 2018; Raposeiro et al., 2021; Sear et al.,  
417 2020; Vachula et al., 2019, 2020). This method has detected the arrival of Viking settlers in other Nordic regions, such as in  
418 the Lofoten islands in northern Norway (D'Anjou et al., 2012, Fig. 9B) and in the Faeroe Islands (Curtin et al., 2021, Fig. 9C).  
419 However, SVID sterol/stanol records show no evident human signals at or around the time of colonisation (i.e., 9<sup>th</sup> century CE,  
420 ca 1.1 ka BP). While a relative maximum of sterol/stanol concentrations found at ca 1.4 ka BP resembles the timing of an  
421 earlier-than-colonisation stanol signal found in the Faeroes (Curtin et al., 2021), as well as an analogous signal in the Lofoten  
422 Islands (D'Anjou et al., 2012), we cannot confidently interpret this peak as indication of human presence as its amplitude is  
423 comparable in magnitude to the inherent variability in the record (i.e., low signal to noise ratio).



424

425 **Figure 9:** Holocene sub-Arctic records of faecal stanols in North Atlantic Islands. (A) 5 $\beta$ -stigmastanol (dark red) and sum of  
426 coprostanol and epi-coprostanol (dark blue) from core 20-SVID-02, NE Iceland (this study); (B) 5 $\beta$ -stigmastanol (pink) and  
427 coprostanol (light blue) from cores LILA09-LILC09 from Lilandsvatnet lake, Lofoten Islands (D'Anjou et al., 2012); (C) 5 $\beta$ -  
428 stigmastanol (orange) and coprostanol + epi-coprostanol (green) from core EI-D-01-15 from Eiðisvatn lake, Faeroe Islands (Curtin  
429 et al., 2021).



430 The lack of a clear anthropogenic faecal biomarker signal could be explained by either (1) a scarce/null incidence of human  
431 activities in the catchment (unlikely, given the archaeological evidence in nearby areas; Gísladóttir et al., 2012; Lebrun et al.,  
432 2023) and/or by (2) dilution of the signal due to the relatively large size of the lake paired to a small catchment. The sterol/stanol  
433 records show a general increase throughout the Holocene (Fig. A2) in a pattern that matches the C/N, *n*-alkanes and perylene  
434 trends, suggesting that the primary driver of SVID's sterol signal is likely landscape instability and soil erosion rather than  
435 human/ruminant presence. Furthermore, ratios of sterols to their derived 5 $\beta$ -5 $\alpha$  stanols can trace redox conditions in various  
436 environments (e.g. Andersson and Meyers, 2012; Canuel and Martens, 1993; Jaffé et al., 1996; Routh et al., 2014) and thus,  
437 potentially, human presence in a lake catchment, as anthropogenic activities tend to mobilise more soil and increase in-wash  
438 of organic material, fostering reducing conditions (Argiriadis et al., 2018). In SVID, the stanol values (5 $\beta$ -5 $\alpha$ ) are consistently  
439 lower than their respective sterol precursors, suggesting a generally oxidising environment throughout the Holocene (Fig. 6).  
440 The only exception to this trend is in the earliest part of the record (ca 10.8–10.6 ka BP; Fig. 5), indicative of a more reducing  
441 environment, though not linked to an increased organic input (low TC values), but more likely to lake stratification with  
442 deglacial water sinking at the bottom of the lake (Sugiyama et al., 2021).

### 443 6.3 Holocene fire frequency

444 Pyrogenic PAHs are considered a reliable proxy for fire frequency on a local scale, within and around a catchment (Denis et  
445 al., 2012). Although other factors can influence the PAH signal in sedimentary archives (e.g., accumulation rates, degradation;  
446 Stogiannidis et al., 2015), we interpret SVID pyroPAHs data as a record of NE Iceland fire history through the Holocene.

447 The trend in pyroPAHs does not match the erosional signal described by bulk geochemical proxies and *n*-alkanes, suggesting  
448 that soil erosion is not a mechanism for Holocene pyroPAHs variability. We exclude chemical degradation as a source of the  
449 signal, as PAHs are relatively stable molecules on long time scales (e.g., Johnsen et al., 2005). In fact, the ratio between low  
450 molecular weight (more prone to chemical degradation and leeching) and high molecular weight PAHs (as defined in Fig. A5)  
451 remains above 1 in most samples. Similarly, the pyrene/coronene ratio shows high and stable values throughout the record,  
452 indicating good preservation, with no significant degradation or preferential removal of less recalcitrant PAHs such as pyrene  
453 (Fig. A5 and refs therein).

454 The pyroPAH record presents two peaks at ca 2.8 and 1.5 ka BP, both predating acknowledged human settlement. PyroPAH  
455 values subsequently drop (VIII) and increase again in the last two centuries reaching maximum values in the present (Fig. 7A).  
456 Analysing PAH data subdivided in molecular weight classes (see 4.1; Table A1; Fig. 7B) can help explain these two features  
457 as well as the general trend. HMW pyroPAHs show low and stable relative contributions (12 $\pm$ 7% of total pyroPAHs) through  
458 the whole record and rise to 70% in the last 200 years. This trend, paired with increased pyroPAH concentrations, is consistent  
459 with the burning of coal/oil, the use of internal combustion engines, and increased human presence (Abas and Mohamad, 2011;  
460 Kozak et al., 2017). MMW pyroPAHs show relatively stable concentrations through most of the record (until ca 0.2 ka BP).  
461 Their relative abundance (~68 $\pm$ 35%) slowly decreases through the Holocene, proportionally to the increase of LMW  
462 pyroPAHs (~20 $\pm$ 16%). The latter, which are predominantly present in the gaseous phase (Karp et al., 2020), peak at 3–2.8 and  
463 1.5 ka BP, and substantially control the shape of the pyroPAH record (Fig. 7A-B). Together, the (1) low and stable values of  
464 HMW pyroPAHs, the (2) stable MMW values, and the (3) increasing/peaking values of LMW pyroPAHs are consistent with  
465 a general increase in the frequency of low temperature fires (e.g., peat fires or crawling fires) at a regional level. While the  
466 Hekla 3 event (3.01 ka BP, the largest rhyolitic eruption during the Holocene; Larsen, 1977; Larsen and Eiríksson, 2008)  
467 occurs just before the first pyroPAH peak, it is unlikely to be its unique or even main cause. The effects of tephra fallout on  
468 vegetation and related PAH deposition, seem to be quite short lived, with fires events likely coeval to the eruption and  
469 vegetation recovering within a few decades (Eddudóttir et al., 2017; Pickarski et al., 2023). The deposition of volcanic sourced  
470 PAHs also tends to be temporally confined to the eruption year and consist mainly of MMW PAHs (Kozak et al., 2017), while  
471 SVID pyroPAH peaks are clearly led by increases in LMW PAHs on a longer timescale. Notably, this shift in fire regime at



472 ca 3 ka BP in Iceland falls within a wider pattern of increasing fire frequency emerging from the analysis of several Holocene  
473 fire records throughout Europe (Marlon et al., 2013). This is linked to either an increase of cultivated land (fire was used to  
474 clear land for agriculture) and/or, particularly in Europe, to increasing aridity (Marlon et al., 2013). We hypothesize that the  
475 latter is the most probable explanation for the shifts in NE Icelandic fire regimes as discussed in Section 5.4.

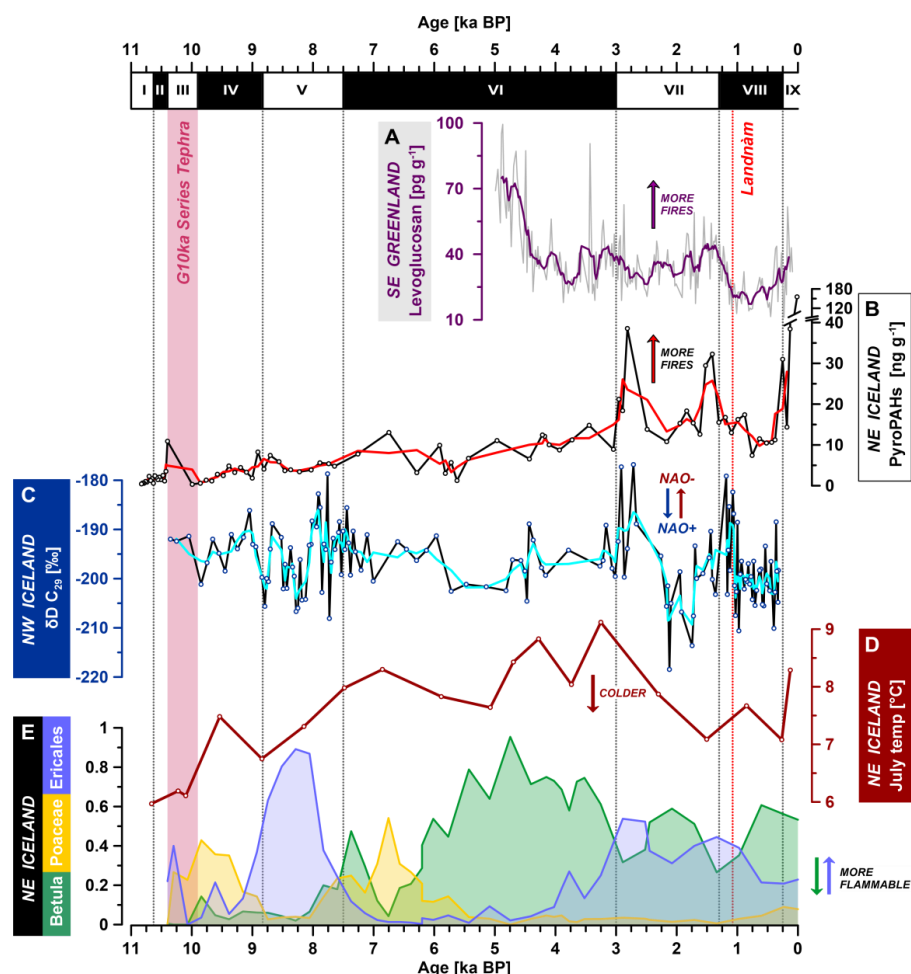
#### 476 **6.4 Regional drivers of precipitation and their role on fire frequency**

477 Fuel moisture content and, more generally, environmental moisture, are the main variables controlling flammability in  
478 vegetational communities typical of temperate/sub-arctic regions (Marino et al., 2010; Plucinski et al., 2010; Santana and  
479 Marrs, 2014). The North Atlantic Oscillation (NAO; Hurrell et al., 2003) modulates the intensity of the westerly storm track  
480 and thus the amount and source of precipitation in Iceland. Its positive mode (NAO+) brings intervals of higher precipitation  
481 resulting in a wetter (and often warmer) climate than NAO- intervals, which are characterised by weaker westerlies, stronger  
482 northerly winds, and drier (and often colder) conditions (Hurrell, 1995; Trouet et al., 2009). Major changes in precipitation  
483 regimes usually lead to changes in the hydrogen stable isotopic value of environmental water ( $\delta D$ ; Dansgaard, 1964) which  
484 translate into shifts in the  $\delta D$  of plant waxes (e.g., *n*-alkanes; Sachse et al., 2012). This relationship has been calibrated in  
485 various environments, including the Arctic (e.g., Berke et al., 2019; Bush et al., 2017; McFarlin et al., 2019; Thomas et al.,  
486 2016) and applied for paleo-precipitation reconstructions (e.g., Ardenghi et al., 2019; Niedermeyer et al., 2016; Tierney et al.,  
487 2017; Wilkie et al., 2013). A  $C_{29}$  *n*-alkane  $\delta D$  record from a fjord core in NW Iceland (Fig. 10C; Moossen et al., 2015) describes  
488 a relatively stable NAO+ configuration (wetter - more D-depleted) throughout the Holocene, and two major shifts toward  
489 NAO- (drier - less D-depleted) conditions at ca 3–2.5 and 1.5–1.0 ka BP, matching the timing of first SVID pyroPAH peak  
490 and at least partially overlapping to the second one. A similar correlation of fire frequency shifts to NAO- configurations has  
491 recently been suggested for other Arctic sites, particularly in Svalbard (Chen et al., 2023).

492 Biomass typology (i.e., the kind of vegetation on site) also influences fuel flammability (Chandler et al., 1983; Fernandes and  
493 Cruz, 2012; Santana et al., 2011; Scarff and Westoby, 2006). In Iceland, many plant taxa appeared shortly after deglaciation  
494 (e.g., Alsos et al., 2021). Increasing summer temperatures led to the expansion of thermophilic woody plant taxa (e.g., birch)  
495 during/after the Holocene Thermal Maximum (e.g., Eddudóttir et al., 2016; Geirsdóttir et al., 2022; Karlsdóttir et al., 2014).  
496 Since ~6 ka BP, the birch woodland in the NE region has evolved into more open heathland and peatland, until the birch  
497 population decreased around 3 ka BP (Roy et al., 2018), along with a general temperature decrease (Axford et al., 2007). In  
498 this context, at Ytra-Áland (Fig. 1B), two major drops in *Betula* pollen coeval to two increases in Ericales (heather's order)  
499 pollen closely follow the NAO- shifts at 3 and 1.5 ka BP (Fig. 10E; Karlsdóttir et al., 2014). Heathlands, especially in low  
500 moisture conditions, are associated with higher flammability, particularly high sustainability (i.e., how well the combustion  
501 proceeds). Thus, heathlands are prone to longer, more stable fires, and with an increased potential for igniting higher canopy  
502 elements and underlying peat layers (Plucinski et al., 2010; Rein et al., 2008; Santana and Marrs, 2014). More frequent, more  
503 stable, slow crawling fires involving dense bushes and peat would increase the amount of pyroPAHs produced and deposited  
504 in the region while skewing their distribution toward LMW components (George et al., 2016; Inuma et al., 2007; Siao et al.,  
505 2007), as observed in the SVID pyroPAH signal (Fig. 7). Lastly, the observed shifts in pyroPAHs are unlikely to be the result  
506 of a change in their source area. Our back-trajectory analysis reveals that more air parcels originate over Iceland or in the  
507 surrounding North Atlantic (Fig. 8). The analysis further reveals that trajectories with terrestrial origins are more likely in  
508 NAO+ than NAO- regimes. As such terrestrial trajectories would be the ones responsible for bringing combustion products to  
509 SVID, we might therefore expect a stronger pyroPAH signal during NAO+ intervals. However, our results display the opposite  
510 trend, with the initial increase in pyroPAH abundances at ~3 ka occurring during an NAO- mode and their subsequent drop  
511 occurring during a strong NAO+ interval. Thus, the late Holocene increase in pyroPAHs in SVID is likely to record a  
512 substantial increase in local fires (driven by vegetation change and NAO-modulated aridity) rather than a shift in the  
513 compounds' sources.



514 Overall, SVID pyroPAH signal describes a major shift from a relatively stable (i.e., low fire frequency) early and mid-Holocene  
515 environment to a dryer late-Holocene environment at ca 3 ka BP, naturally more prone to long term persistence of low  
516 temperature wildfires. This is likely the result of the combination of (1) recorded cooling and related shifts in vegetational  
517 communities, (2) NAO- shifts and associated dryer conditions.



518

519 **Figure 10: Regional comparison of climatic, fire, and vegetation records.** (A, purple) levoglucosan concentrations from the RECAP  
520 ice core, south-eastern Greenland (Segato et al., 2021); (B, black) sum of pyrogenic PAHs concentrations – red line indicates a 3  
521 points running average; (C, blue) stable isotopic composition of hydrogen of sedimentary *n*-alkanes from marine core MD99-2266  
522 off the coast of NW Iceland (Moossen et al., 2015) – cyan line indicates a 3 points running average; (D, red) chronomid derived  
523 temperatures from core 04-SVID-03 (Axford et al., 2007); (E) pollen percentages of *Betula* (green), *Poaceae* (yellow), and *Ericales*  
524 (blue) in a peat section from the Ytra-Áland site, NE Iceland (Karlsdóttir et al., 2014).

## 525 6.5 Evidence for a human influence on fire frequency?

526 Unlike other proxies, pyroPAHs return to background levels after reaching high values at 1.5 ka BP, and then remain low  
527 through the Medieval Warm Period (ca 900–1200 CE) and most of the Little Ice Age (1300–1900 CE), before peaking again  
528 in the last 150–200 years. A similar drop in fire markers (anhydrosugars) is also observed in eastern Greenland (Segato et al.,  
529 2021; Fig. 10A). Low pyroPAHs levels during an interval of known human presence in Iceland suggests that human activities  
530 might have curbed regional fire frequency, thus modulating the natural signal, which would have otherwise remained relatively  
531 high due to the persistence of colder conditions and more flammable plant communities (regardless of NAO shifts). In fact,  
532 while increased pressure from grazing lowered environmental resilience to soil erosion (e.g., Bates et al., 2021; Eddudóttir et



533 al., 2016; McGovern et al., 2007), it likely also decreased fuel flammability (which is dependent on the amount of dead  
534 biomass; Davies and Legg, 2011; Santana and Marrs, 2014) in the predominant heathland environment (Lake et al., 2001).  
535 Additionally, the creation of farmland and pastureland at the expenses of areas with woody vegetation and heathland likely  
536 reduced the extent of the biomes naturally prone to fires. This reduction of local wood availability is reflected in changes of  
537 foraging habits, as settlers shifted to relying more heavily on more abundant fuel sources such as peat and turf, as well as other  
538 marine derived substances (e.g., seal oil, seaweed; Bold, 2012), while driftwood and imported wood (from Europe or North  
539 America, often with ad hoc expeditions) satisfied most of the need for timber (e.g., Bold, 2012; Edvardsson, 2010; Mooney,  
540 2016; Pinta, 2021; Sveinbjarnardóttir et al., 2007). A general mechanism for fire suppression due to the expansion of cultivated  
541 land has already been proposed for global data (Marlon et al., 2013), but assumed to be likely asynchronous in different regions  
542 and strongly influenced by local climatic, environmental, and social conditions.  
543 We speculate that the drop in fire markers in Iceland from the reduction in wildfire risk due to husbandry and farming exceeded  
544 the production of fire markers due to human necessities (e.g., warming), resulting in an overall suppressed fire signal. This  
545 would also be consistent with the low population density, which started to increase only in the 1800s CE (Iceland Statistical  
546 Service, 2023; Jónsson and Magnússon, 1997), matching the coldest interval of the Little Ice Age and the sharp rise in HMW  
547 pyroPAHs. From this perspective, the pressure of human activities would have fostered erosion through decreased  
548 environmental resilience while, at the same time, suppressing natural fire frequency.

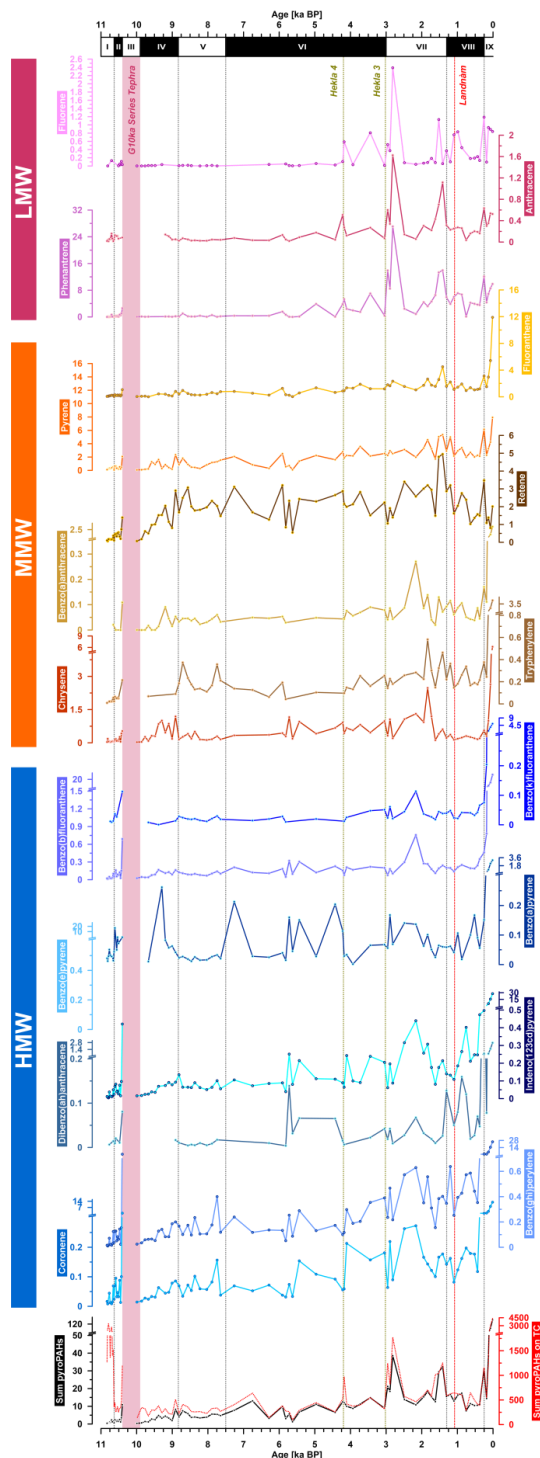
## 549 7 Conclusions

550 Our multiproxy analysis of Holocene sediments from Stóra Viðarvatn provides new insight into the coupled vegetation, fire,  
551 erosion, and climate regimes of NE Iceland:

- 552 • Bulk geochemistry proxies show that the general climatic evolution of NE Iceland is primarily driven by summer  
553 insolation: an initial deglacial warming followed by a relatively warm and stable climate until ca 4–3 ka BP, after which  
554 declining summer temperatures result in accelerating catchment erosion.
- 555 • Faecal biomarkers, traditionally linked to human activities, do not show an elevated signal at or around colonisation (9<sup>th</sup>  
556 century CE). Instead, faecal biomarkers roughly trace the erosional signal described by bulk geochemical proxies. This  
557 may result from a combination of (1) low local anthropogenic pressure (although sparse settlements existed a few km  
558 from the study area), and (2) signal dilution, due to the large lake size and its relatively small watershed. Therefore, we  
559 urge caution when interpreting faecal biomarkers as unequivocal proxies of human presence, particularly when highly  
560 sensitive analytical tools like the one used in this study are involved.
- 561 • PyroPAHs carry a regional (mostly confined to northern and north-eastern Iceland) and predominantly natural signal  
562 (i.e., controlled by parameters such as precipitation and moisture availability, vegetation typology and flammability).  
563 After generally low fire frequency throughout most of the Holocene, we observe major regime changes at 3 ka and 1.5  
564 ka BP, before known human colonisation in Iceland. During this interval, the distribution of pyroPAHs point toward a  
565 regional increase in low temperature fire frequency. This can be linked to a change in vegetation typology driven by the  
566 cooling of the last 4 to 3 kyr, coupled to major shifts in atmospheric circulation (i.e., NAO regimes) that led to increased  
567 aridity and thus flammability. Finally, low levels of pyroPAHs characterise the time following known human  
568 colonisation, before rising again (but with a molecular composition more distinctive of fossil fuels) in the last ~200 years.  
569 This suggests that human activities, particularly husbandry and farming, may have suppressed fire frequency by reducing  
570 the range and flammability of environments more prone to fire, effectively modulating the natural signal while decreasing  
571 the resilience of the local environment to soil erosion.

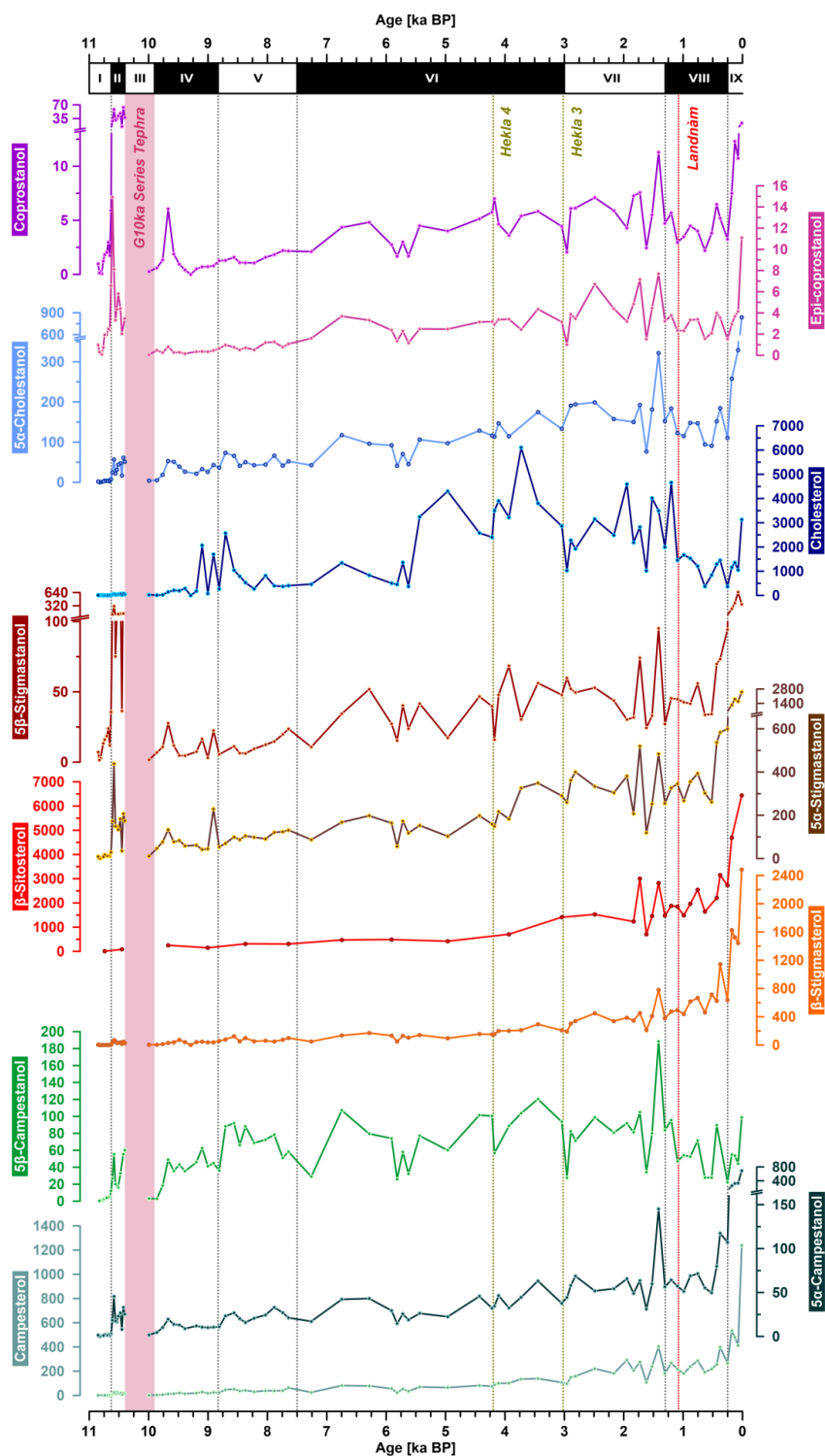


572 8 Appendices



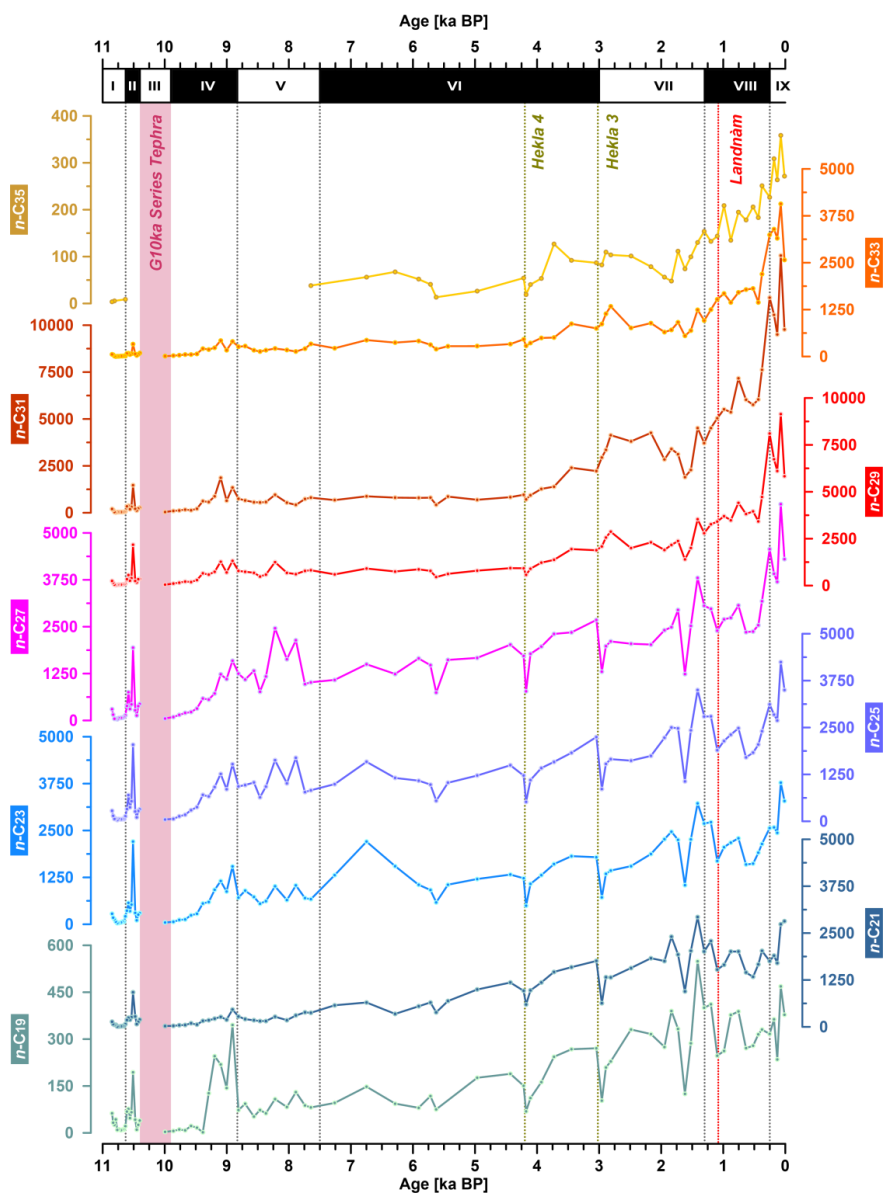
573  
574 **Figure A1:** Concentration curves of all 20-SVID-02 pyrogenic PAHs recovered in this study. All concentrations are expressed as ng  
575 per g of dry sample, except for the last curve (red-dotted) which is in ng per g of TC. Note that several vertical axes have been  
576 adjusted to minimise the rise in the last 2–3 centuries. Compounds are listed in chromatographic order and grouped by molecular  
577 weight through colour shading (LMW in red purple; MMW in yellow orange; HMW in blue).





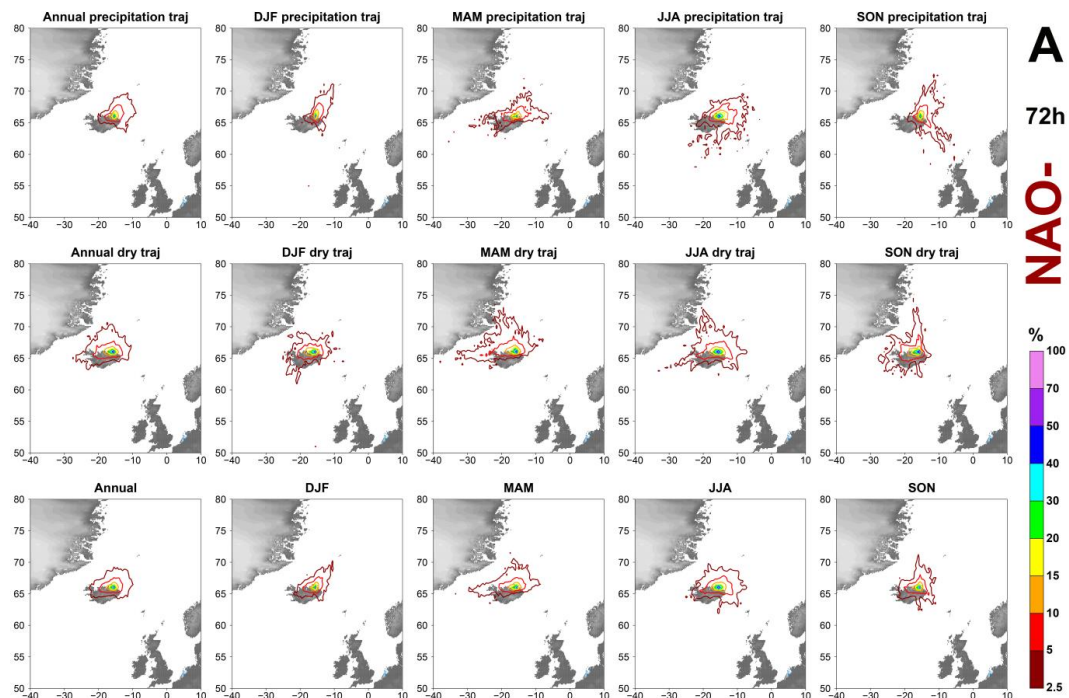
578

579 **Figure A2:** Concentration curves of all 20-SVID-02 faecal sterol/stanols of interest recovered in this study. All concentrations are  
580 expressed as ng per g of dry sample. Note that several vertical axes have been adjusted to minimise the rise in the last 2–3 centuries.  
581 Compounds are grouped and colour shaded by structure (cholesterol and stanol derivatives in blue purple; sito-stigma-  
582 sterols and stanols in red orange; campestanol and campestanol in green).

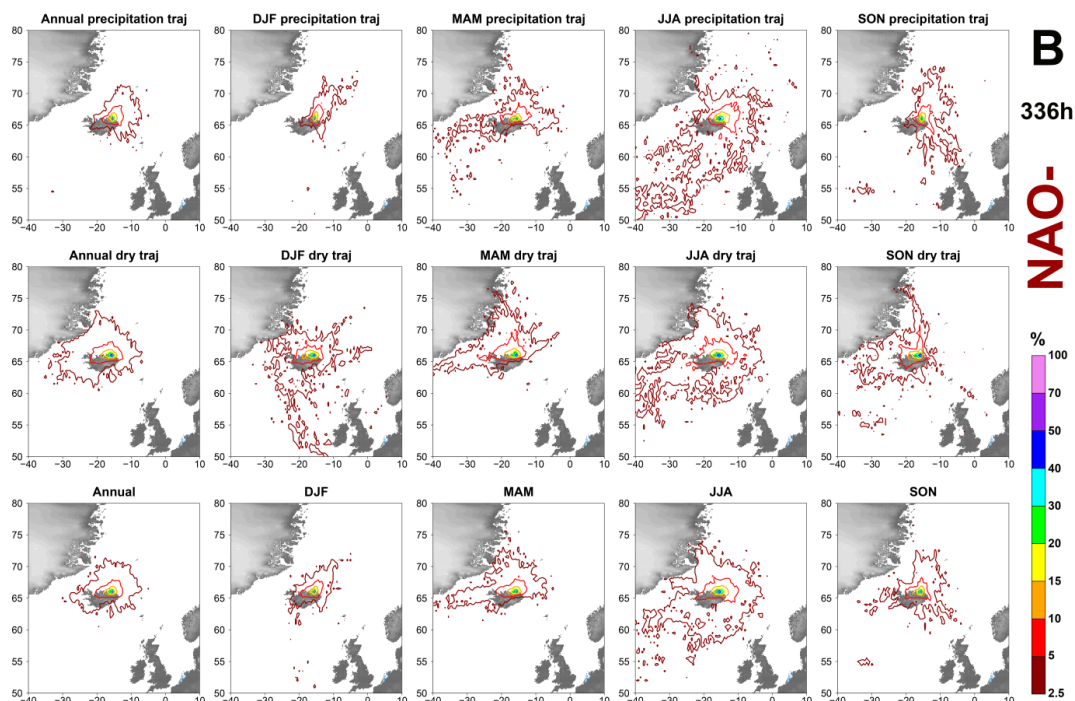


583

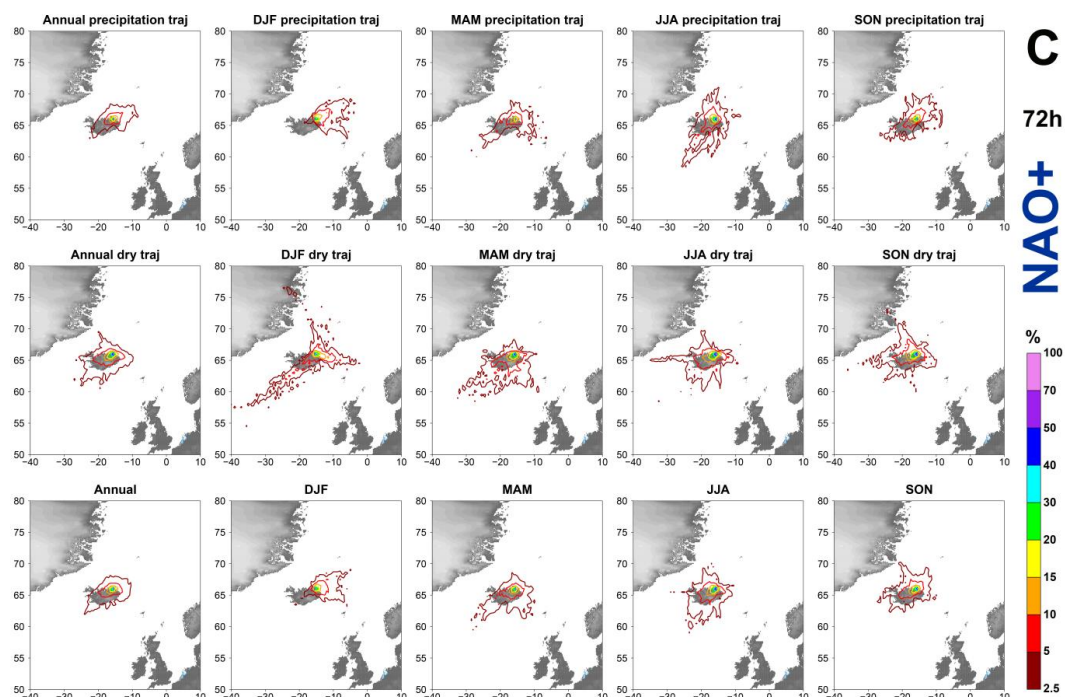
584 **Figure A3:** Concentration curves of all 20-SVID odd-numbered *n*-alkane homologues from *n*-C<sub>19</sub> to *n*-C<sub>35</sub> recovered in this study.  
585 All concentrations are expressed as ng per g of dry sample.



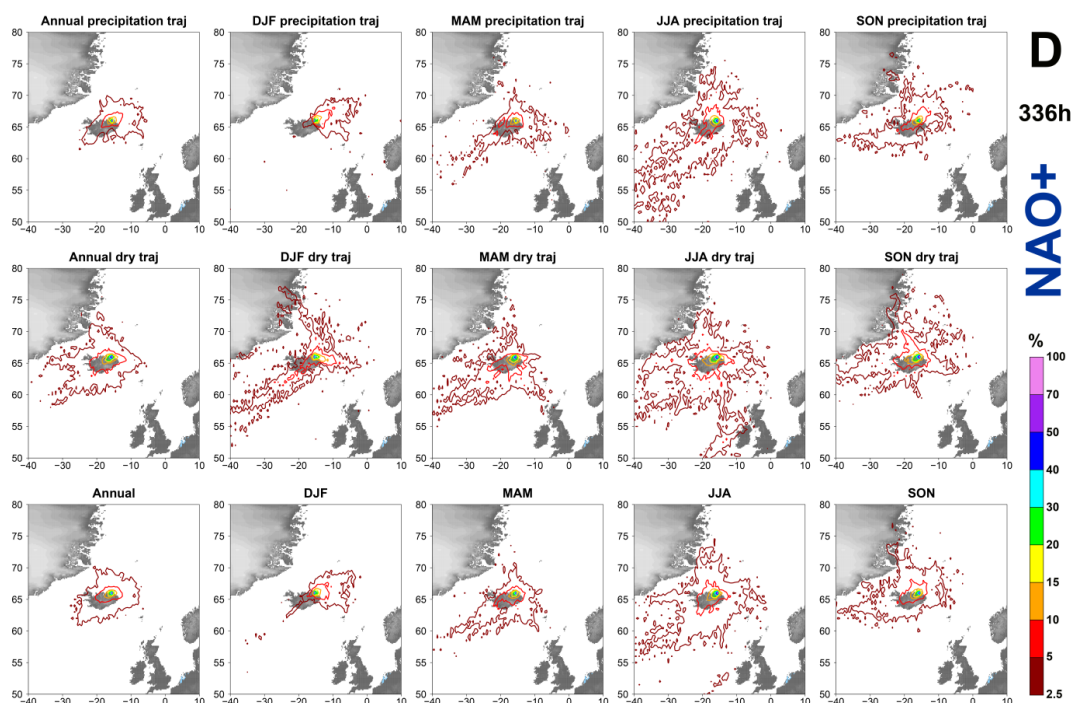
586



587

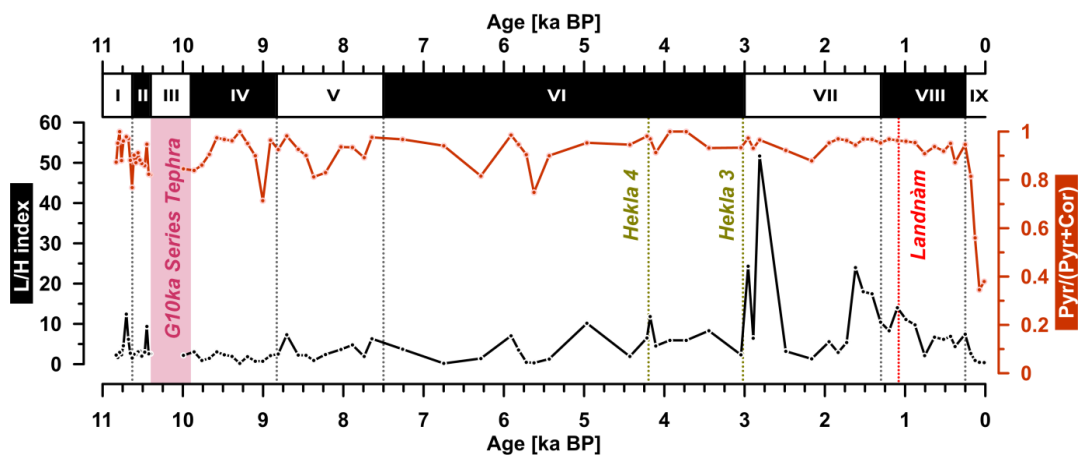


588



589

590 **Figure A4:** HYSPLIT back trajectories of air parcels for December 2009 to November 2010 (NAO-) and May 2013 to April 2014  
591 (NAO+, except for October 2014). Trajectories are calculated on a three days (72 h, A-C) and a two weeks (336 h, B-D)  
592 intervals at a 6 hours frequency; “precipitation” (top) indicates trajectories that produced precipitation within 6 h from the SVID endpoint,  
593 “dry” (middle) vice versa; bottom plots are the sum of “precipitation” and “dry” trajectories. Contour colours indicate the frequency  
594 at which air parcels part of a trajectory travel above a certain area.



595

596

Figure A5: PAH indices used as an indication of PAH preservation.

597

The L/H index (black) is a ratio between low and high molecular weight unsubstituted PAHs, defined as  $L/H = (\text{Phenanthrene} + \text{Anthracene} + \text{Fluoranthene} + \text{Pyrene}) / (\text{Benzo}[a]\text{anthracene} + \text{Chrysene} + \text{Benzo}[k]\text{fluoranthene} + \text{Benzo}[a]\text{pyrene} + \text{Indeno}[1,2,3,c,d]\text{pyrene} + \text{Dibenzo}[a,h]\text{anthracene} + \text{Benzo}[g,h,i]\text{perylene})$  (Magi et al., 2002; Stogiannidis et al., 2015 and refs. therein).

599

600

The Pyrene-Coronene index (orange) defined as  $\text{pyrene} / (\text{pyrene} + \text{coronene})$  is based on the assumption of a higher preservation potential of the HMW coronene over the lighter, more soluble pyrene (Denis, 2016; Denis et al., 2017; May et al., 1978); higher, more stable values point toward good preservation for both HMW and LMW PAHs.

601

602

603



604 **Table A1: Polycyclic aromatic hydrocarbons (PAHs) analysed in this study. Pyrogenic PAHs are grouped into low, medium, and**  
 605 **high molecular weight. Elution order and SRM transitions are reported for each compound.**  
 606

Elution order	Group	Compound name	Mass	Product mass a/b	Collision energy
1		Naphthalene*	128	128/102	8
2		Acenaphthylene*	152	152	8
3	LMW	Acenaphthene*	154	153/154	8
4		Fluorene	166	166	8
5		Phenanthrene	178	178	8
6		Anthracene	178	178	8
7		Fluoranthene	202	202	8
8		Pyrene	202	202	8
11	MMW	Retene	234	234/219	8
12		Benzo[a]anthracene	228	228	8
13		Triphenylene	228	228	8
14		Chrysene	228	228	8
15		Benzo[k]fluoranthene	252	252	8
16		Benzo[j]fluoranthene	252	252	8
17	HMW	Benzo[a]pyrene	252	252	8
19		Indeno[1,2,3-C,D]pyrene	276	276	8
20		Dibenzo[a,h]anthracene	278	278	8
21		Benzo[g,h,i]perylene	276	276	8
22		Coronene	300	300	8
18		Perylene**	252	252	8
9		p-Terphenyl D14 (IS)	244	244	8
10		p-Terphenyl (IS)	230	230	8

\* Compound(s) difficult to quantify correctly and thus excluded from final sums.

\*\* Non-pyrogenic PAH.

607



608 **Table A2: Faecal sterols and stanols analysed in this study. Elution order and SRM transitions are reported for each compound.**  
 609

Elution order	Name	Detailed name	CAS #	Quantitative qualitative	Mass	Product Mass	Collision Energy
1	Pregnanol (IS)	5 $\beta$ -pregnan-3 $\alpha$ -ol	4352-07-2	Q	361	215	10
				q	361	191	10
2	5 $\alpha$ -Cholestane (IS)	5 $\alpha$ -cholestane	481-21-0	Q	372	217	10
				q			
3	Coprostanol	5 $\beta$ -cholestan-3 $\beta$ -ol	360-68-9	Q	370	215	10
				q	460	215	10
4	Epi-Coprostanol	5 $\beta$ -cholestan-3 $\alpha$ -ol	516-92-7	Q	370	215	10
				q	460	215	10
5	Cholesterol	5-en-cholest-3 $\beta$ -ol	57-88-5	Q	368	145	20
				q	458	129	50
6	Cholestanol	5 $\alpha$ -cholestan-3 $\beta$ -ol	80-97-7	Q	370	215	10
				q	460	215	10
7	5 $\beta$ -Campestanol	24R-methyl-5 $\beta$ -cholestan-3 $\beta$ -ol	33947-18-1	Q	384	215	10
				q	474	215	10
8	5 $\beta$ -Stigma(sito)stanol	24R-ethyl-5 $\beta$ -cholestan-3 $\beta$ -ol	4736-91-8	Q	383	147	20
				q	488	215	10
9	Campesterol	24R-methyl-5-en-cholest-3 $\beta$ -ol	474-62-4	Q	382	255	5
				q	472	129	50
10	5 $\alpha$ -Campestanol	24R-methyl-5 $\alpha$ -cholestan-3 $\beta$ -ol	474-60-2	Q	384	215	10
				q	474	215	10
11	$\beta$ -Stigmasterol	24S-ethyl-5,22E-dien-cholest-3 $\beta$ -ol	83-48-7	Q	394	255	5
				q	484	211	20
12	$\beta$ -Sitosterol	24R-ethyl-5-en-cholest-3 $\beta$ -ol	83-46-5	Q	396	255	10
				q	484	394	10
13	5 $\alpha$ -Stigma(sito)stanol	24R-ethyl-5 $\alpha$ -cholestan-3 $\beta$ -ol	83-45-4	Q	383	147	20
				q	488	215	10

610



611 **9 Data availability**

612 All raw data will be available on the NOAA National Centers for Environmental Information  
613 (<https://www.ncei.noaa.gov/access/paleo-search/study/38503>).  
614 The data will also be made available upon request.

615 **10 Author contributions**

616 GHM, ÁG and JS conceptualized research and obtained financial support for the NSF project ILLUME (Iceland landscape  
617 reconstruction using molecular proxies); GHM, ÁG, JHR, DJH, and NA participated in the field campaign to retrieve the  
618 sediment core; JS and GHM provided laboratory and analytical infrastructure; NA, DJH, and BRH processed all sediment  
619 samples; NA performed method development and sample analysis. TT and DJH performed the tephra analysis and developed  
620 the age model; NA performed the HYSPLIT analysis; NA wrote the manuscript draft, except for the age model paragraph  
621 (DJH); GHM, ÁG, JS, DJH, and JHR reviewed and edited the manuscript.

622 **11 Competing interests**

623 The authors declare that they have no conflict of interest.

624 **12 Acknowledgements**

625 We kindly thank Sveinbjörn Steinþórsson and Þór Blöndahl for lake coring assistance at Stóra Viðarvatn. We thank Dr. Jamie  
626 McFarlin (INSTAAR and University of Wyoming), Dr. Nadia Dildar (INSTAAR), Dr. Sebastian Kopf (INSTAAR), and  
627 Katelyn Eaman for their invaluable analytical support in the lab; Dr. Thomas Marchitto (INSTAAR) for providing access to  
628 the clean room used for sampling; Jeremy Caves Rugestein (Colorado State University) for sharing his expertise on  
629 HYSPLIT; and Karl Painter and Isaiah Castro for helping with biogenic silica analyses.

630 **13 Financial support**

631 This work was supported by the National Science Foundation grant ARC1836981 to GHM, ÁG, JS, and TT, and by a  
632 University of Iceland grant to ÁG.





633 **14 References**

- 634 Abas, M. R. B. and Mohamad, S.: Hazardous (Organic) Air Pollutants, *Encycl. Environ. Heal.*, 23–33,  
635 <https://doi.org/10.1016/B978-0-444-52272-6.00070-2>, 2011.
- 636 Aizenshtat, Z.: Perylene and its geochemical significance, *Geochim. Cosmoc. Acta*, 37, 559–567,  
637 [https://doi.org/10.1016/0016-7037\(73\)90218-4](https://doi.org/10.1016/0016-7037(73)90218-4), 1973.
- 638 Alsos, I. G., Lammers, Y., Kjellman, S. E., Merkel, M. K. F., Bender, E. M., Rouillard, A., Erlendsson, E., Guðmundsdóttir,  
639 E. R., Benediktsson, Í. Ö., Farnsworth, W. R., Brynjólfsson, S., Gísladóttir, G., Eddudóttir, S. D., and Schomacker, A.: Ancient  
640 sedimentary DNA shows rapid post-glacial colonisation of Iceland followed by relatively stable vegetation until the Norse  
641 settlement (Landnám) AD 870, *Quat. Sci. Rev.*, 259, <https://doi.org/10.1016/j.quascirev.2021.106903>, 2021.
- 642 Andersson, R. A. and Meyers, P. A.: Effect of climate change on delivery and degradation of lipid biomarkers in a Holocene  
643 peat sequence in the Eastern European Russian Arctic, *Org. Geochem.*, 53, 63–72,  
644 <https://doi.org/10.1016/j.orggeochem.2012.05.002>, 2012.
- 645 Ardenghi, N., Mulch, A., Koutsodendris, A., Pross, J., Kahmen, A., and Niedermeyer, E. M.: Temperature and moisture  
646 variability in the eastern Mediterranean region during Marine Isotope Stages 11–10 based on biomarker analysis of the Tenaghi  
647 Philippon peat deposit, *Quat. Sci. Rev.*, 225, 105977, <https://doi.org/https://doi.org/10.1016/j.quascirev.2019.105977>, 2019.
- 648 Arellano, L., Fernández, P., Van Drooge, B. L., Rose, N. L., Nickus, U., Thies, H., Stuchlík, E., Camarero, L., Catalan, J., and  
649 Grimalt, J. O.: Drivers of atmospheric deposition of polycyclic aromatic hydrocarbons at European high-altitude sites, *Atmos.*  
650 *Chem. Phys.*, 18, 16081–16097, <https://doi.org/10.5194/acp-18-16081-2018>, 2018.
- 651 Argiriadis, E., Battistel, D., McWethy, D. B., Vecchiato, M., Kirchgeorg, T., Kehrwald, N. M., Whitlock, C., Wilmshurst, J.  
652 M., and Barbante, C.: Lake sediment fecal and biomass burning biomarkers provide direct evidence for prehistoric human-lit  
653 fires in New Zealand, *Sci. Rep.*, 8, <https://doi.org/10.1038/s41598-018-30606-3>, 2018.
- 654 Axford, Y., Miller, G. H., Geirsdóttir, Á., and Langdon, P. G.: Holocene temperature history of northern Iceland inferred from  
655 subfossil midges, *Quat. Sci. Rev.*, 26, 3344–3358, <https://doi.org/10.1016/j.quascirev.2007.09.003>, 2007.
- 656 Ayris, P. M. and Delmelle, P.: The immediate environmental effects of tephra emission, *Bull. Volcanol.*, 74, 1905–1936,  
657 <https://doi.org/10.1007/s00445-012-0654-5>, 2012.
- 658 Bates, R., Erlendsson, E., Eddudóttir, S. D., Möckel, S. C., Tinganelli, L., and Gísladóttir, G.: Landnám , Land Use and  
659 Landscape Change at Kagaðarhóll in Northwest Iceland , *Environ. Archaeol.*, 0, 1–17,  
660 <https://doi.org/10.1080/14614103.2021.1949680>, 2021.
- 661 Battistel, D., Argiriadis, E., Kehrwald, N., Spigariol, M., Russell, J. M., and Barbante, C.: Fire and human record at Lake  
662 Victoria, East Africa, during the Early Iron Age: Did humans or climate cause massive ecosystem changes?, *Holocene*, 27,  
663 997–1007, <https://doi.org/10.1177/0959683616678466>, 2016.
- 664 Berger, A. and Loutre, M.-F.: Parameters of the Earths orbit for the last 5 Million years in 1 kyr resolution,  
665 <https://doi.org/10.1594/PANGAEA.56040>, 1999.
- 666 Berke, M. A., Sierra, A. C., Bush, R. T., Cheah, D., and O’Connor, K.: Controls on leaf wax fractionation and  $\delta^2\text{H}$  values in  
667 tundra vascular plants from western Greenland, *Geochim. Cosmoc. Acta*, 244, 565–583,  
668 <https://doi.org/https://doi.org/10.1016/j.gca.2018.10.020>, 2019.
- 669 Bershaw, J., Penny, S. M., and Garziona, C. N.: Stable isotopes of modern water across the Himalaya and eastern Tibetan  
670 Plateau: Implications for estimates of paleoelevation and paleoclimate, *J. Geophys. Res. Atmos.*, 117, 1–18,  
671 <https://doi.org/10.1029/2011JD016132>, 2012.
- 672 Birk, J. J., Dippold, M., Wiesenberg, G. L. B., and Glaser, B.: Combined quantification of faecal sterols, stanols, stanones and  
673 bile acids in soils and terrestrial sediments by gas chromatography-mass spectrometry, *J. Chromatogr. A*, 1242, 1–10,  
674 <https://doi.org/10.1016/j.chroma.2012.04.027>, 2012.
- 675 Blaauw, M. and Christeny, J. A.: Flexible paleoclimate age-depth models using an autoregressive gamma process, Bayesian



- 676 Anal., 6, 457–474, <https://doi.org/10.1214/11-BA618>, 2011.
- 677 Bold, R.: Norse Utilisation of Archaeobotanical Resources within the Myvatnssveit locale, Northern Iceland, PhD thesis,  
678 Durham University, <http://etheses.dur.ac.uk/3440/>, 2012.
- 679 Bray, E. E. and Evans, E. D.: Distribution of *n*-paraffins as a clue to recognition of source beds, *Geochim. Cosmoc. Acta*, 22,  
680 2–15, [https://doi.org/10.1016/0016-7037\(61\)90069-2](https://doi.org/10.1016/0016-7037(61)90069-2), 1961.
- 681 Bronk Ramsey, C., Albert, P. G., Blockley, S. P. E., Hardiman, M., Housley, R. A., Lane, C. S., Lee, S., Matthews, I. P.,  
682 Smith, V. C., and Lowe, J. J.: Improved age estimates for key Late Quaternary European tephra horizons in the RESET lattice,  
683 *Quat. Sci. Rev.*, 118, 18–32, <https://doi.org/10.1016/j.quascirev.2014.11.007>, 2015.
- 684 Bull, I. D., Evershed, R. P., and Betancourt, P. P.: An organic geochemical investigation of the practice of manuring at a  
685 Minoan site on Pseira Island, Crete, *Geoarchaeology*, 16, 223–242, [https://doi.org/10.1002/1520-6548\(200102\)16:2<223::AID-GEA1002>3.0.CO;2-7](https://doi.org/10.1002/1520-6548(200102)16:2<223::AID-GEA1002>3.0.CO;2-7), 2001.
- 687 Bull, I. D., Lockheart, M. J., Elhmmali, M. M., Roberts, D. J., and Evershed, R. P.: The origin of faeces by means of biomarker  
688 detection, *Environ. Int.*, 27, 647–654, [https://doi.org/10.1016/S0160-4120\(01\)00124-6](https://doi.org/10.1016/S0160-4120(01)00124-6), 2002.
- 689 Bush, R. T., Berke, M. A., and Jacobson, A. D.: Plant Water  $\delta$ D and  $\delta^{18}$ O of Tundra Species from West Greenland, Arctic,  
690 *Antarct. Alp. Res.*, 49, 341–358, <https://doi.org/10.1657/AAAR0016-025>, 2017.
- 691 Callegaro, A., Battistel, D., Kehrwald, N. M., Matsubara Pereira, F., Kirchgeorg, T., Del Carmen Villoslada Hidalgo, M., Bird,  
692 B. W., and Barbante, C.: Fire, vegetation, and Holocene climate in a southeastern Tibetan lake: A multi-biomarker  
693 reconstruction from Paru Co, *Clim. Past*, 14, 1543–1563, <https://doi.org/10.5194/cp-14-1543-2018>, 2018.
- 694 Canuel, E. A. and Martens, C. S.: Seasonal variations in the sources and alteration of organic matter associated with recently-  
695 deposited sediments, *Org. Geochem.*, 20, 563–577, [https://doi.org/10.1016/0146-6380\(93\)90024-6](https://doi.org/10.1016/0146-6380(93)90024-6), 1993.
- 696 Caves Rugenstein, J. K. and Chamberlain, C. P.: The evolution of hydroclimate in Asia over the Cenozoic: A stable-isotope  
697 perspective, *Earth-Science Rev.*, 185, 1129–1156, <https://doi.org/10.1016/j.earscirev.2018.09.003>, 2018.
- 698 Chandler, C., Cheney, P., Thomas, P., Trabaud, L., and Williams, D.: Fire in forestry. Volume 1. Forest fire behavior and  
699 effects. Volume 2. Forest fire management and organization., John Wiley & Sons, Inc., 1983.
- 700 Chen, A., Yang, L., Sun, L., Gao, Y., and Xie, Z.: Holocene changes in biomass burning in the boreal Northern Hemisphere,  
701 reconstructed from anhydrosugar fluxes in an Arctic sediment profile, *Sci. Total Environ.*, 867, 161460,  
702 <https://doi.org/10.1016/j.scitotenv.2023.161460>, 2023.
- 703 Colman, S. M., Peck, J. A., Karabanov, E. B., Carter, S. J., Bradbury, J. P., King, J. W., and Williams, D. F.: Continental  
704 climate response to orbital forcing from biogenic silica records in lake Baikal, *Nature*, 378, 769–771,  
705 <https://doi.org/10.1038/378769a0>, 1995.
- 706 Conley, D. J.: Biogenic silica as an estimate of siliceous microfossil abundance in Great Lakes sediments, *Biogeochemistry*,  
707 6, 161–179, <https://doi.org/10.1007/BF02182994>, 1988.
- 708 Conley, D. J. and Schelske, C. L.: Biogenic silica, in: Tracking environmental change using lake sediments, edited by: Last,  
709 W. M. and Smol, J. P., Springer Science & Business Media, 281–293, ISBN 1402006284, 2002.
- 710 Cordeiro, L. G. S. M., Carreira, R. S., and Wagener, A. L. R.: Geochemistry of fecal sterols in a contaminated estuary in  
711 southeastern Brazil, *Org. Geochem.*, 39, 1097–1103, <https://doi.org/10.1016/j.orggeochem.2008.02.022>, 2008.
- 712 Curtin, L., D’Andrea, W. J., Balascio, N. L., Shirazi, S., Shapiro, B., de Wet, G. A., Bradley, R. S., and Bakke, J.: Sedimentary  
713 DNA and molecular evidence for early human occupation of the Faroe Islands, *Commun. Earth Environ.*, 2,  
714 <https://doi.org/10.1038/s43247-021-00318-0>, 2021.
- 715 D’Anjou, R. M., Bradley, R. S., Balascio, N. L., and Finkelstein, D. B.: Climate impacts on human settlement and agricultural  
716 activities in northern Norway revealed through sediment biogeochemistry, *Proc. Natl. Acad. Sci. U. S. A.*, 109, 20332–20337,  
717 <https://doi.org/10.1073/pnas.1212730109>, 2012.
- 718 Dansgaard, W.: Stable isotopes in precipitation, *Tellus*, 16, 436–468, <https://doi.org/10.3402/tellusa.v16i4.8993>, 1964.



- 719 Davies, G. M. and Legg, C. J.: Fuel Moisture Thresholds in the Flammability of *Calluna vulgaris*, *Fire Technol.*, 47, 421–436,  
720 <https://doi.org/10.1007/s10694-010-0162-0>, 2011.
- 721 Denis, E. H.: Production and preservation of organic and fire-derived carbon across the Paleocene-Eocene Thermal Maximum,  
722 PhD thesis, Pennsylvania State University, [https://etda.libraries.psu.edu/files/final\\_submissions/12576](https://etda.libraries.psu.edu/files/final_submissions/12576), 2016.
- 723 Denis, E. H., Toney, J. L., Tarozo, R., Scott Anderson, R., Roach, L. D., and Huang, Y.: Polycyclic aromatic hydrocarbons  
724 (PAHs) in lake sediments record historic fire events: Validation using HPLC-fluorescence detection, *Org. Geochem.*, 45, 7–  
725 17, <https://doi.org/10.1016/j.orggeochem.2012.01.005>, 2012.
- 726 Denis, E. H., Pedentchouk, N., Schouten, S., Pagani, M., and Freeman, K. H.: Fire and ecosystem change in the Arctic across  
727 the Paleocene–Eocene Thermal Maximum, *Earth Planet. Sci. Lett.*, 467, 149–156, <https://doi.org/10.1016/j.epsl.2017.03.021>,  
728 2017.
- 729 Dion-Kirschner, H., McFarlin, J. M., Masterson, A. L., Axford, Y., and Osburn, M. R.: Modern constraints on the sources and  
730 climate signals recorded by sedimentary plant waxes in west Greenland, *Geochim. Cosmoc. Acta*, 286, 336–354,  
731 <https://doi.org/10.1016/j.gca.2020.07.027>, 2020.
- 732 Draxler, R. R., Hess, G. D., and Draxler R. R., and Hess G., D.: An overview of the HYSPLIT\_4 modelling system for  
733 trajectories, *Aust. Meteorol. Mag.*, 47, 295–308, 1998.
- 734 Duan, Y., Wu, Y., Cao, X., Zhao, Y., and Ma, L.: Hydrogen isotope ratios of individual *n*-alkanes in plants from Gannan Gahai  
735 Lake (China) and surrounding area, *Org. Geochem.*, 77, 96–105, <https://doi.org/10.1016/j.orggeochem.2014.10.005>, 2014.
- 736 Dugmore, A. J., Shore, J. S., Cook, G. T., Newton, A. J., Edwards, K. J., and Larsen, G.: The radiocarbon dating of tephra  
737 layers in Britain and Iceland, 15th Int. C Conf., 37, 379–388, 1995.
- 738 Eddudóttir, S. D., Erlendsson, E., Tinganelli, L., and Gísladóttir, G.: Climate change and human impact in a sensitive  
739 ecosystem: the Holocene environment of the Northwest Icelandic highland margin, *Boreas*, 45, 715–728,  
740 <https://doi.org/10.1111/bor.12184>, 2016.
- 741 Eddudóttir, S. D., Erlendsson, E., and Gísladóttir, G.: Effects of the Hekla 4 tephra on vegetation in Northwest Iceland, *Veg.*  
742 *Hist. Archaeobot.*, 26, 389–402, <https://doi.org/10.1007/s00334-017-0603-5>, 2017.
- 743 Eddudóttir, S. D., Erlendsson, E., and Gísladóttir, G.: An Icelandic terrestrial record of North Atlantic cooling c. 8800–8100  
744 cal. yr BP, *Quat. Sci. Rev.*, 197, 246–256, <https://doi.org/10.1016/j.quascirev.2018.07.017>, 2018.
- 745 Edvardsson, R.: The role of marine resources in the medieval economy of Vestfirðir, Iceland, PhD thesis, University of New  
746 York, UMI Number: 3396427, 2010.
- 747 Eglinton, G. and Hamilton, R. J.: Leaf epicuticular waxes, *Science* (80-. ), 156, 1322–1335,  
748 <https://doi.org/10.1126/science.156.3780.1322>, 1967.
- 749 Esri: ArcGIS Pro (Version 3.1.0); Earthstar Geographic “World Imagery” map, accessed March 2023.,  
750 <https://doi.org/https://www.arcgis.com/home/item.html?id=10df2279f9684e4a9f6a7f08febac2a9>, 2023.
- 751 Evershed, R. P., Bethell, P. H., Reynolds, P. J., and Walsh, N. J.: 5 $\beta$ -Stigmastanol and related 5 $\beta$ -stanols as biomarkers of  
752 manuring: analysis of modern experimental material and assessment of the archaeological potential, *J. Archaeol. Sci.*, 24, 485–  
753 495, <https://doi.org/10.1006/jasc.1996.0132>, 1997.
- 754 Feng, D., Liu, Y., Gao, Y., Zhou, J., Zheng, L., Qiao, G., Ma, L., Lin, Z., and Grathwohl, P.: Atmospheric bulk deposition of  
755 polycyclic aromatic hydrocarbons in Shanghai: Temporal and spatial variation, and global comparison, *Environ. Pollut.*, 230,  
756 639–647, <https://doi.org/10.1016/j.envpol.2017.07.022>, 2017.
- 757 Fernandes, P. M. and Cruz, M. G.: Plant flammability experiments offer limited insight into vegetation-fire dynamics  
758 interactions, *New Phytol.*, 194, 606–609, <https://doi.org/10.1111/j.1469-8137.2012.04065.x>, 2012.
- 759 Fernández-Martínez, M., Preece, C., Corbera, J., Cano, O., Garcia-Porta, J., Sardans, J., Janssens, I. A., Sabater, F., and  
760 Peñuelas, J.: Bryophyte C: N: P stoichiometry, biogeochemical niches and elementome plasticity driven by environment and  
761 coexistence, *Ecol. Lett.*, 24, 1375–1386, 2021.



- 762 Ficken, K. J., Li, B., Swain, D. L., and Eglinton, G.: An *n*-alkane proxy for the sedimentary input of submerged/floating  
763 freshwater aquatic macrophytes, *Org. Geochem.*, 31, 745–749, [https://doi.org/10.1016/S0146-6380\(00\)00081-4](https://doi.org/10.1016/S0146-6380(00)00081-4), 2000.
- 764 Flowers, G. E., Björnsson, H., Geirsdóttir, Á., Miller, G. H., Black, J. L., and Clarke, G. K. C.: Holocene climate conditions  
765 and glacier variation in central Iceland from physical modelling and empirical evidence, *Quat. Sci. Rev.*, 27, 797–813,  
766 <https://doi.org/10.1016/j.quascirev.2007.12.004>, 2008.
- 767 Gagosian, R. B. and Peltzer, E. T.: The importance of atmospheric input of terrestrial organic material to deep sea sediments,  
768 *Org. Geochem.*, 10, 661–669, [https://doi.org/http://dx.doi.org/10.1016/S0146-6380\(86\)80002-X](https://doi.org/http://dx.doi.org/10.1016/S0146-6380(86)80002-X), 1986.
- 769 Geirsdóttir, Á., Miller, G. H., Thordarson, T., and Ólafsdóttir, K. B.: A 2000 year record of climate variations reconstructed  
770 from Haukadalssvatn, West Iceland, *J. Paleolimnol.*, 41, 95–115, <https://doi.org/10.1007/s10933-008-9253-z>, 2009a.
- 771 Geirsdóttir, Á., Miller, G. H., Axford, Y., and Ólafsdóttir, S.: Holocene and latest Pleistocene climate and glacier fluctuations  
772 in Iceland, *Quat. Sci. Rev.*, 28, 2107–2118, <https://doi.org/10.1016/j.quascirev.2009.03.013>, 2009b.
- 773 Geirsdóttir, Á., Miller, G. H., Larsen, D. J., and Ólafsdóttir, S.: Abrupt holocene climate transitions in the northern North  
774 Atlantic region recorded by synchronized lacustrine records in Iceland, *Quat. Sci. Rev.*, 70, 48–62,  
775 <https://doi.org/10.1016/j.quascirev.2013.03.010>, 2013.
- 776 Geirsdóttir, Á., Miller, G. H., Andrews, J. T., Harning, D. J., Anderson, L. S., Florian, C., Larsen, D. J., and Thordarson, T.:  
777 The onset of neoglaciation in Iceland and the 4.2 ka event, *Clim. Past*, 15, 25–40, <https://doi.org/10.5194/cp-15-25-2019>, 2019.
- 778 Geirsdóttir, Á., Harning, D. J., Miller, G. H., Andrews, J. T., Zhong, Y., and Caseldine, C.: Holocene history of landscape  
779 instability in Iceland: Can we deconvolve the impacts of climate, volcanism and human activity?, *Quat. Sci. Rev.*, 249,  
780 <https://doi.org/10.1016/j.quascirev.2020.106633>, 2020.
- 781 Geirsdóttir, Á., Miller, G. H., Harning, D. J., Hannesdóttir, H., Thordarson, T., and Jónsdóttir, I.: Recurrent outburst floods  
782 and explosive volcanism during the Younger Dryas–Early Holocene deglaciation in south Iceland: evidence from a lacustrine  
783 record, *J. Quat. Sci.*, 37, 1006–1023, <https://doi.org/10.1002/jqs.3344>, 2022.
- 784 George, I. J., Black, R. R., Geron, C. D., Aurell, J., Hays, M. D., Preston, W. T., and Gullett, B. K.: Volatile and semivolatile  
785 organic compounds in laboratory peat fire emissions, *Atmos. Environ.*, 132, 163–170,  
786 <https://doi.org/10.1016/j.atmosenv.2016.02.025>, 2016.
- 787 Gísladóttir, G., Woollett, J. M., Hébert, C. D., and Newton, A.: The Svalbarð project, *Archaeol. Islandica*, 10, 65–103, ISSN  
788 1560-8026, 2012.
- 789 Goad, L.: The Biosynthesis of Plant Sterols, 146–168, [https://doi.org/10.1007/978-3-642-66632-2\\_8](https://doi.org/10.1007/978-3-642-66632-2_8), 1977.
- 790 Goad, L. and Goodwin, T.: The biosynthesis of sterols in higher plants, *Biochem. J.*, 99, 735–746,  
791 <https://doi.org/10.1042/bj0990735>, 1966.
- 792 Goldammer, J. G. and Furyaev, V. V.: Fire in ecosystems of boreal Eurasia: Ecological impacts and links to the global system,  
793 *Fire Ecosyst. Boreal Eurasia*, 1–20, 1996.
- 794 Golomb, D., Barry, E., Fisher, G., Varanusupakul, P., Koleda, M., and Rooney, T.: Atmospheric deposition of polycyclic  
795 aromatic hydrocarbons near New England coastal waters, *Atmos. Environ.*, 35, 6245–6258, [https://doi.org/10.1016/S1352-2310\(01\)00456-3](https://doi.org/10.1016/S1352-2310(01)00456-3), 2001.
- 797 Grimalt, J. and Albaigés, J.: Source and occurrence of C<sub>12</sub>–C<sub>22</sub> *n*-alkane distributions with even carbon-number preference in  
798 sedimentary environments, *Geochim. Cosmochim. Acta*, 51, 1379–1384, [https://doi.org/10.1016/0016-7037\(87\)90322-X](https://doi.org/10.1016/0016-7037(87)90322-X), 1987.
- 799 Gross, M.: An investigation of paleo-wildfires during the Cretaceous–Paleogene (K–PG) boundary at El Kef, Tunisia,  
800 Undergraduate Honors thesis, University of Colorado, Boulder, [https://scholar.colorado.edu/honr\\_theses/1351](https://scholar.colorado.edu/honr_theses/1351), 2017.
- 801 Guo, J. and Liao, H.: In-situ formation of perylene in lacustrine sediments and its geochemical significance, *Acta Geochim.*,  
802 39, 587–594, <https://doi.org/10.1007/s11631-020-00400-y>, 2020.
- 803 Iceland Statistical Service: <https://www.hagstofa.is/>, last access: 13 March 2023.
- 804 Halsall, C. J., Sweetman, A. J., Barrie, L. A., and Jones, K. C.: Modelling the behaviour of PAHs during atmospheric transport



- 805 from the UK to the Arctic, *Atmos. Environ.*, 35, 255–267, [https://doi.org/10.1016/S1352-2310\(00\)00195-3](https://doi.org/10.1016/S1352-2310(00)00195-3), 2001.
- 806 Han, J. and Calvin, M.: Hydrocarbon distribution of algae and bacteria, and microbiological activity in sediments, *Proc. Natl.*  
807 *Acad. Sci.*, 64, 436–443, 1969.
- 808 Hanke, U. M., Lima-Braun, A. L., Eglinton, T. I., Donnelly, J. P., Galy, V., Poussart, P., Hughen, K., McNichol, A. P., Xu,  
809 L., and Reddy, C. M.: Significance of perylene for source allocation of terrigenous organic matter in aquatic sediments,  
810 *Environ. Sci. Technol.*, 53, 8244–8251, <https://doi.org/10.1021/acs.est.9b02344>, 2019.
- 811 Harning, D. J., Geirsdóttir, Á., Miller, G. H., and Zalzal, K.: Early Holocene deglaciation of Drangajökull, Vestfirðir, Iceland,  
812 *Quat. Sci. Rev.*, 153, 192–198, <https://doi.org/10.1016/j.quascirev.2016.09.030>, 2016.
- 813 Harning, D. J., Thordarson, T., Geirsdóttir, Á., Zalzal, K., and Miller, G. H.: Provenance, stratigraphy and chronology of  
814 Holocene tephra from Vestfirðir, Iceland, *Quat. Geochronol.*, 46, 59–76, <https://doi.org/10.1016/j.quageo.2018.03.007>, 2018a.
- 815 Harning, D. J., Geirsdóttir, Á., and Miller, G. H.: Punctuated Holocene climate of Vestfirðir, Iceland, linked to internal/external  
816 variables and oceanographic conditions, *Quat. Sci. Rev.*, 189, 31–42, <https://doi.org/10.1016/j.quascirev.2018.04.009>, 2018b.
- 817 Harning, D. J., Curtin, L., Geirsdóttir, Á., D’Andrea, W. J., Miller, G. H., and Sepúlveda, J.: Lipid Biomarkers Quantify  
818 Holocene Summer Temperature and Ice Cap Sensitivity in Icelandic Lakes, *Geophys. Res. Lett.*, 47,  
819 <https://doi.org/10.1029/2019GL085728>, 2020.
- 820 Harning, D. J., Jennings, A. E., Köseoglu, D., Belt, S. T., Geirsdóttir, Á., and Sepúlveda, J.: Response of biological productivity  
821 to North Atlantic marine front migration during the Holocene, *Clim. Past*, 17, 379–396, [https://doi.org/10.5194/cp-17-379-](https://doi.org/10.5194/cp-17-379-2021)  
822 2021, 2021.
- 823 Hatcher, P. G. and McGillivray, P. A.: Sewage Contamination in the New York Bight. Coprostanol as an Indicator, *Environ.*  
824 *Sci. Technol.*, 13, 1225–1229, <https://doi.org/10.1021/es60158a015>, 1979.
- 825 He, D., Zhang, K., Tang, J., Cui, X., and Sun, Y.: Using fecal sterols to assess dynamics of sewage input in sediments along a  
826 human-impacted river-estuary system in eastern China, *Sci. Total Environ.*, 636, 787–797,  
827 <https://doi.org/10.1016/j.scitotenv.2018.04.314>, 2018.
- 828 Hernández, A., Bao, R., Giralt, S., Barker, P. A., Leng, M. J., Sloane, H. J., and Sáez, A.: Biogeochemical processes controlling  
829 oxygen and carbon isotopes of diatom silica in Late Glacial to Holocene lacustrine rhythmites, *Palaeogeogr. Palaeoclimatol.*  
830 *Palaeoecol.*, 299, 413–425, <https://doi.org/10.1016/j.palaeo.2010.11.020>, 2011.
- 831 Hiles, W., Lawson, I. T., Roucoux, K. H., and Streeter, R. T.: Late survival of woodland contrasts with rapid limnological  
832 changes following settlement at Kalmantjörn, Mývatnssveit, northeast Iceland, *Boreas*, 50, 1209–1227,  
833 <https://doi.org/10.1111/bor.12529>, 2021.
- 834 Hoffmann, D. and Wynder, E. L.: Organic particulate pollutants: Chemical analysis and bioassays for carcinogenicity, in: *Air*  
835 *pollution*, vol. II, Academic Press New York, 67–95, ISBN 0-12-666602-4, 1977.
- 836 Hollister, K. V., Thomas, E. K., Reynolds, M. K., Bültmann, H., Raberg, J. H., Miller, G. H., and Sepúlveda, J.: Aquatic and  
837 terrestrial plant contributions to sedimentary plant waxes in a modern arctic lake setting, *J. Geophys. Res. Biogeosc.*, 127,  
838 <https://doi.org/https://doi.org/10.1029/2022JG006903>, 2022.
- 839 Hurrell, J. W.: Decadal trends in the North Atlantic Oscillation: Regional Temperatures and Precipitation, *Science*, 269, 676–  
840 679, <https://doi.org/10.1126/science.269.5224.676>, 1995.
- 841 Hurrell, J. W., Kushnir, Y., Otterson, G., and Visbeck, M.: An Overview of the North Atlantic Oscillation, *North Atl. Oscil.*  
842 *Clim. Significance Environ. Impact*, 134, 263, <https://doi.org/10.1029/GM134>, 2003.
- 843 Ifkirne, M., Beri, Q., Schaefer, A., Pham, Q. B., Acharki, S., and Farah, A.: Study of the impact of ash fallout from the Icelandic  
844 volcano Eyjafjöll (2010) on vegetation using MODIS data, *Nat. Hazards*, 1–21, <https://doi.org/10.1007/s11069-022-05544-z>,  
845 2022.
- 846 Iinuma, Y., Brüggemann, E., Gnauk, T., Müller, K., Andreae, M. O., Helas, G., Parmar, R., and Herrmann, H.: Source  
847 characterization of biomass burning particles: The combustion of selected European conifers, African hardwood, savanna



- 848 grass, and German and Indonesian peat, *J. Geophys. Res. Atmos.*, 112, <https://doi.org/10.1029/2006JD007120>, 2007.
- 849 Jaffé, R., Cabrera, A., Hajje, N., and Carvajal-Chitty, H.: Organic biogeochemistry of a hypereutrophic tropical, freshwater  
850 lake - Part 1: particle associated and dissolved lipids, *Org. Geochem.*, 25, 227–240, [https://doi.org/10.1016/S0146-](https://doi.org/10.1016/S0146-6380(96)00114-3)  
851 [6380\(96\)00114-3](https://doi.org/10.1016/S0146-6380(96)00114-3), 1996.
- 852 Jennings, A., Thordarson, T., Zalzal, K., Stoner, J., Hayward, C., Geirsdóttir, Á., and Miller, G. H.: Holocene tephra from  
853 Iceland and Alaska in SE Greenland shelf sediments, *Geol. Soc. London, Spec. Publ.*, 398, 157–193,  
854 <https://doi.org/10.1144/SP398.6>, 2014.
- 855 Jiang, C., Alexander, R., Kagi, R. I., and Murray, A. P.: Origin of perylene in ancient sediments and its geological significance,  
856 *Org. Geochem.*, 31, 1545–1559, [https://doi.org/10.1016/S0146-6380\(00\)00074-7](https://doi.org/10.1016/S0146-6380(00)00074-7), 2000.
- 857 Johnsen, A. R., Wick, L. Y., and Harms, H.: Principles of microbial PAH-degradation in soil, *Environ. Pollut.*, 133, 71–84,  
858 <https://doi.org/10.1016/j.envpol.2004.04.015>, 2005.
- 859 Jónsson, G. and Magnússon, M. S.: *Hagskinna: Icelandic historical statistics*, Stat. Iceland, Reykjavík, Icel., 1997.
- 860 Junk, G. A. and Ford, C. S.: Review of organic emissions from selected combustion processes, Ames Lab., IA (USA), 1980.
- 861 Karlsdóttir, L., Hallsdóttir, M., Eggertsson, Ó., Thorssón, Æ. T., and Anamthawat-Jónsson, K.: Birch hybridization in  
862 Thistilfjörður, North-east Iceland during the Holocene, *Icelandic Agric. Sci.*, 27, 95–109, ISSN 1670-567X, 2014.
- 863 Karp, A. T., Holman, A. I., Hopper, P., Grice, K., and Freeman, K. H.: Fire distinguishers: Refined interpretations of polycyclic  
864 aromatic hydrocarbons for paleo-applications, *Geochim. Cosmoc. Acta*, 289, 93–113,  
865 <https://doi.org/10.1016/j.gca.2020.08.024>, 2020.
- 866 Kaushal, S. and Binford, M. W.: Relationship between C:N ratios of lake sediments, organic matter sources, and historical  
867 deforestation in Lake Pleasant, Massachusetts, USA, *J. Paleolimnol.*, 22, 439–442, <https://doi.org/10.1023/A:1008027028029>,  
868 1999.
- 869 Kilian, R., Biester, H., Behrmann, J., Baeza, O., Fesq-Martin, M., Hohner, M., Schimpf, D., Friedmann, A., and Mangini, A.:  
870 Millennium-scale volcanic impact on a superhumid and pristine ecosystem, *Geology*, 34, 609–612,  
871 <https://doi.org/10.1130/G22605.1>, 2006.
- 872 Kozak, K., Ruman, M., Kosek, K., Karasiński, G., Stachnik, Ł., and Polkowska, Z.: Impact of volcanic eruptions on the  
873 occurrence of PAHs compounds in the aquatic ecosystem of the southern part of West Spitsbergen (Hornsund Fjord, Svalbard),  
874 *Water (Switzerland)*, 9, <https://doi.org/10.3390/w9010042>, 2017.
- 875 Lake, S., Bullock, J. M., and Hartley, S.: Impacts of livestock grazing on lowland heathland in the UK, *English Nat. Res.*  
876 *Reports*, 422, 143, ISSN 0967-876X, 2001.
- 877 Lammel, G., Sehili, A. M., Bond, T. C., Feichter, J., and Grassl, H.: Gas/particle partitioning and global distribution of  
878 polycyclic aromatic hydrocarbons - A modelling approach, *Chemosphere*, 76, 98–106,  
879 <https://doi.org/10.1016/j.chemosphere.2009.02.017>, 2009.
- 880 Larsen, D. J., Miller, G. H., Geirsdóttir, Á., and Thordarson, T.: A 3000-year varved record of glacier activity and climate  
881 change from the proglacial lake Hvítárvatn, Iceland, *Quat. Sci. Rev.*, 30, 2715–2731,  
882 <https://doi.org/10.1016/j.quascirev.2011.05.026>, 2011.
- 883 Larsen, D. J., Miller, G. H., Geirsdóttir, Á., and Ólafsdóttir, S.: Non-linear Holocene climate evolution in the North Atlantic:  
884 A high-resolution, multi-proxy record of glacier activity and environmental change from Hvítárvatn, central Iceland, *Quat.*  
885 *Sci. Rev.*, 39, 14–25, <https://doi.org/10.1016/j.quascirev.2012.02.006>, 2012.
- 886 Larsen, G.: H4 and other acid Hekla tephra layers, *Jokull*, 27, 28–46, <https://timarit.is/gegnir/000527808>, 1977.
- 887 Larsen, G. and Eiríksson, J.: Late Quaternary terrestrial tephrochronology of Iceland—frequency of explosive eruptions, type  
888 and volume of tephra deposits, *J. Quat. Sci. Publ. Quat. Res. Assoc.*, 23, 109–120, <https://doi.org/10.1002/jqs.1129>, 2008.
- 889 Larsen, G., Eiríksson, J., Knudsen, K. L., and Heinemeier, J.: Correlation of late Holocene terrestrial and marine tephra  
890 markers, north Iceland: Implications for reservoir age changes, *Polar Res.*, 21, 283–290, [38](https://doi.org/10.1111/j.1751-</a></p></div><div data-bbox=)



- 891 8369.2002.tb00082.x, 2002.
- 892 Lebrun, J., Bhiry, N., Woollett, J., and Sæmundsson, Þ.: Slope Dynamics in Relation to the Occupation and Abandonment of  
893 a Mountain Farm in Þistilfjörður, Northeast Iceland, *Geosciences*, 13, 30, <https://doi.org/10.3390/geosciences13020030>, 2023.
- 894 Lechler, A. R. and Galewsky, J.: Refining paleoaltimetry reconstructions of the Sierra Nevada: California, using air parcel  
895 trajectories, *Geology*, 41, 259–262, <https://doi.org/10.1130/G33553.1>, 2013.
- 896 Leeming, R., Ball, A., Ashbolt, N., and Nichols, P.: Using faecal sterols from humans and animals to distinguish faecal  
897 pollution in receiving waters, *Water Res.*, 30, 2893–2900, [https://doi.org/10.1016/S0043-1354\(96\)00011-5](https://doi.org/10.1016/S0043-1354(96)00011-5), 1996.
- 898 Leeming, R. L., Ball, A., Ashbolt, N. J., Jones, G., and Nichols, P. D.: Distinguishing between human and animal sources of  
899 faecal pollution., 61, <http://hdl.handle.net/102.100.100/237154?index=1>, 1994.
- 900 Lerch, M., Bromm, T., Geitner, C., Haas, J. N., Schäfer, D., Glaser, B., and Zech, M.: Human and livestock faecal biomarkers  
901 at the prehistorical encampment site of Ullafelsen in the Fotsch Valley , Stubai Alps , Austria - potential and limitations, 1–  
902 24, <https://doi.org/10.5194/bg-2021-186>, 2021.
- 903 Li, C., Ma, S., Xia, Y., He, X., Gao, W., and Zhang, G.: Assessment of the relationship between ACL/CPI values of long chain  
904 *n*-alkanes and climate for the application of paleoclimate over the Tibetan Plateau, *Quat. Int.*, 544, 76–87,  
905 <https://doi.org/10.1016/j.quaint.2020.02.028>, 2020.
- 906 Lima, A. L. C., Farrington, J. W., and Reddy, C. M.: Combustion-Derived Polycyclic Aromatic Hydrocarbons in the  
907 Environment—A Review, *Environ. Forensics*, 6, 109–131, <https://doi.org/10.1080/15275920590952739>, 2005.
- 908 Mack, R. N.: Initial Effects of Ashfall from Mount St. Helens on Vegetation in Eastern Washington and Adjacent Idaho,  
909 *Science*, 213, 537–539, <https://doi.org/10.1126/science.213.4507.537>, 1981.
- 910 Magi, E., Bianco, R., Ianni, C., and Di Carro, M.: Distribution of polycyclic aromatic hydrocarbons in the sediments of the  
911 Adriatic Sea, *Environ. Pollut.*, 119, 91–98, [https://doi.org/10.1016/S0269-7491\(01\)00321-9](https://doi.org/10.1016/S0269-7491(01)00321-9), 2002.
- 912 Marino, E., Madrigal, J., Guijarro, M., Hernando, C., Dez, C., and Fernandez, C.: Flammability descriptors of fine dead fuels  
913 resulting from two mechanical treatments in shrubland: A comparative laboratory study, *Int. J. Wildl. Fire*, 19, 314–324,  
914 <https://doi.org/10.1071/WF08123>, 2010.
- 915 Marlon, J. R.: The geography of fire: A paleo perspective, PhD thesis, University of Oregon, <http://hdl.handle.net/1794/10334>,  
916 2009.
- 917 Marlon, J. R., Bartlein, P. J., Walsh, M. K., Harrison, S. P., Brown, K. J., Edwards, M. E., Higuera, P. E., Power, M. J.,  
918 Anderson, R. S., Briles, C., Brunelle, A., Carcaillet, C., Daniels, M., Hu, F. S., Lavoie, M., Long, C., Minckley, T., Richard,  
919 P. J. H., Scott, A. C., Shafer, D. S., Tinner, W., Umbanhowar, C. E., and Whitlock, C.: Wildfire responses to abrupt climate  
920 change in North America, *Proc. Natl. Acad. Sci. U. S. A.*, 106, 2519–2524, <https://doi.org/10.1073/pnas.0808212106>, 2009.
- 921 Marlon, J. R., Bartlein, P. J., Daniiau, A. L., Harrison, S. P., Maezumi, S. Y., Power, M. J., Tinner, W., and Vanniére, B.:  
922 Global biomass burning: A synthesis and review of Holocene paleofire records and their controls, *Quat. Sci. Rev.*, 65, 5–25,  
923 <https://doi.org/10.1016/j.quascirev.2012.11.029>, 2013.
- 924 Marzi, R., Torkelson, B. E., and Olson, R. K.: A revised carbon preference index, *Org. Geochem.*, 20, 1303–1306,  
925 [https://doi.org/10.1016/0146-6380\(93\)90016-5](https://doi.org/10.1016/0146-6380(93)90016-5), 1993.
- 926 May, W. E., Wasik, S. P., and Freeman, D. H.: Determination of the solubility behavior of some polycyclic aromatic  
927 hydrocarbons in water, *Anal. Chem.*, 23, 877–884, <https://doi.org/10.1021/ac50029a042>, 1978.
- 928 McCalley, D. V., Cooke, M., and Nickless, G.: Effect of sewage treatment on faecal sterols, *Water Res.*, 15, 1019–1025,  
929 [https://doi.org/10.1016/0043-1354\(81\)90211-6](https://doi.org/10.1016/0043-1354(81)90211-6), 1981.
- 930 Mccarty, J. L., Aalto, J., Paunu, V. V., Arnold, S. R., Eckhardt, S., Klimont, Z., Fain, J. J., Evangeliou, N., Venäläinen, A.,  
931 Tchebakova, N. M., Parfenova, E. I., Kupiainen, K., Soja, A. J., Huang, L., and Wilson, S.: Reviews and syntheses: Arctic fire  
932 regimes and emissions in the 21st century, *Biogeosciences*, 18, 5053–5083, <https://doi.org/10.5194/bg-18-5053-2021>, 2021.
- 933 McFarlin, J. M., Axford, Y., Masterson, A. L., and Osburn, M. R.: Calibration of modern sedimentary  $\delta^2\text{H}$  plant wax-water



- 934 relationships in Greenland lakes, *Quat. Sci. Rev.*, 225, 105978, <https://doi.org/10.1016/j.quascirev.2019.105978>, 2019.
- 935 McGovern, T. H., Vésteinsson, O., Friðriksson, A., Church, M., Lawson, I., Simpson, I. A., Einarsson, A., Dugmore, A., Cook,  
936 G., Perdikaris, S., Edwards, K. J., Thomson, A. M., Adderley, W. P., Newton, A., Lucas, G., Edvardsson, R., Aldred, O., and  
937 Dunbar, E.: Landscapes of Settlement in Northern Iceland: Historical Ecology of Human Impact and Climate Fluctuation on  
938 the Millennial Scale, *Am. Anthropol.*, 109, 27–51, <https://doi.org/10.1525/aa.2007.109.1.27>, 2007.
- 939 McGrath, T. E., Chan, W. G., and Hajajigol, R.: Low temperature mechanism for the formation of polycyclic aromatic  
940 hydrocarbons from the pyrolysis of cellulose. *Journal of Analytical and Applied Pyrolysis*, v. 66, p. 51-70, 2003., *J. Anal.*  
941 *Appl. Pyrolysis*, 66, 51–70, 2003.
- 942 McKay, N. P., Kaufman, D. S., and Michelutti, N.: Biogenic silica concentration as a high-resolution, quantitative temperature  
943 proxy at Hallet Lake, south-central Alaska, *Geophys. Res. Lett.*, 35, 4–9, <https://doi.org/10.1029/2007GL032876>, 2008.
- 944 Meyers, P. A.: Preservation of elemental and isotopic source identification of sedimentary organic matter, *Chem. Geol.*, 114,  
945 289–302, [https://doi.org/10.1016/0009-2541\(94\)90059-0](https://doi.org/10.1016/0009-2541(94)90059-0), 1994.
- 946 Meyers, P. A.: Organic geochemical proxies of paleoceanographic, paleolimnologic, and paleoclimatic processes, *Org.*  
947 *Geochem.*, 27, 213–250, [https://doi.org/10.1016/S0146-6380\(97\)00049-1](https://doi.org/10.1016/S0146-6380(97)00049-1), 1997.
- 948 Meyers, P. A. and Ishiwatari, R.: Lacustrine organic geochemistry-an overview of indicators of organic matter sources and  
949 diagenesis in lake sediments, *Org. Geochem.*, 20, 867–900, [https://doi.org/10.1016/0146-6380\(93\)90100-P](https://doi.org/10.1016/0146-6380(93)90100-P), 1993.
- 950 Meyers, P. A. and Teranes, J. L.: Sediment Organic Matter, in: *Tracking Environmental Change Using Lake Sediments:*  
951 *Physical and Geochemical Methods*, edited by: Last, W. M. and Smol, J. P., Springer Netherlands, Dordrecht, 239–269,  
952 [https://doi.org/10.1007/0-306-47670-3\\_9](https://doi.org/10.1007/0-306-47670-3_9), 2001.
- 953 Mjell, T. L., Ninnemann, U. S., Kleiven, H. F., and Hall, I. R.: Multidecadal changes in Iceland Scotland Overflow Water  
954 vigor over the last 600 years and its relationship to climate, *Geophys. Res. Lett.*, 43, 2111–2117,  
955 <https://doi.org/10.1002/2016GL068227>, 2016.
- 956 Mooney, D. E.: Examining Possible Driftwood Use in Viking Age Icelandic Boats, *Nor. Archaeol. Rev.*, 49, 156–176,  
957 <https://doi.org/10.1080/00293652.2016.1211734>, 2016.
- 958 Moossen, H., Bendle, J., Seki, O., Quillmann, U., and Kawamura, K.: North Atlantic Holocene climate evolution recorded by  
959 high-resolution terrestrial and marine biomarker records, *Quat. Sci. Rev.*, 129, 111–127,  
960 <https://doi.org/10.1016/j.quascirev.2015.10.013>, 2015.
- 961 Murtaugh, J. J. and Bunch, R. L.: Sterols as a measure of fecal pollution., *J. Water Pollut. Control Fed.*, 39, 404–409,  
962 <https://www.jstor.org/stable/25035758>, 1967.
- 963 NOAA: <https://www.ncei.noaa.gov/access/monitoring/nao/>, last access: 1 March 2023.
- 964 Niedermeyer, E. M., Forrest, M., Beckmann, B., Sessions, A. L., Mulch, A., and Schefuß, E.: The stable hydrogen isotopic  
965 composition of sedimentary plant waxes as quantitative proxy for rainfall in the West African Sahel, *Geochim. Cosmoc. Acta*,  
966 184, 55–70, <https://doi.org/10.1016/j.gca.2016.03.034>, 2016.
- 967 Norðdahl, H. and Pétursson, H. G.: Relative sea-level changes in Iceland: new aspects of the Weichselian deglaciation of  
968 Iceland, *Dev. Quat. Sci. Elsevier*, 25–78, ISBN 0-444-50652-7, 2005.
- 969 Óladóttir, B. A., Larsen, G., and Sigmarsson, O.: Holocene volcanic activity at Grímsvötn, Bárðarbunga and Kverkfjöll  
970 subglacial centres beneath Vatnajökull, Iceland, *Bull. Volcanol.*, 73, 1187–1208, <https://doi.org/10.1007/s00445-011-0461-4>,  
971 2011.
- 972 Óladóttir, B. A., Thordarson, T., Geirsdóttir, Á., Jóhannsdóttir, G. E., and Mangerud, J.: The Saksunarvatn Ash and the G10ka  
973 series tephra. Review and current state of knowledge, *Quat. Geochronol.*, 56, <https://doi.org/10.1016/j.quageo.2019.101041>,  
974 2020.
- 975 Ólafsdóttir, R., Schlyter, P., and Haraldsson, H. V.: Simulating icelandic vegetation cover during the holocene implications  
976 for long-term land degradation, *Geogr. Ann. Ser. A, Phys. Geogr.*, 83, 203–215, [40](https://doi.org/10.1111/j.0435-</a></p></div><div data-bbox=)





- 977 3676.2001.00155.x, 2001.
- 978 Page, D. S., Boehm, P. D., Douglas, G. S., Bence, A. E., Burns, W. A., and Mankiewicz, P. J.: Pyrogenic polycyclic aromatic  
979 hydrocarbons in sediments record past human activity: A case study in Prince William Sound, Alaska, *Mar. Pollut. Bull.*, 38,  
980 247–260, [https://doi.org/10.1016/S0025-326X\(98\)00142-8](https://doi.org/10.1016/S0025-326X(98)00142-8), 1999.
- 981 Pancost, R. D., Baas, M., Van Geel, B., and Sinninghe Damsté, J. S.: Biomarkers as proxies for plant inputs to peats: An  
982 example from a sub-boreal ombrotrophic bog, *Org. Geochem.*, 33, 675–690, [https://doi.org/10.1016/S0146-6380\(02\)00048-7](https://doi.org/10.1016/S0146-6380(02)00048-7),  
983 2002.
- 984 Patterson, G. W.: Relation between Structure and Retention Time of Sterols in Gas Chromatography, *Anal. Chem.*, 43, 1165–  
985 1170, <https://doi.org/10.1021/ac60304a015>, 1971.
- 986 Petit, T., Lozier, M. S., Josey, S. A., and Cunningham, S. A.: Atlantic Deep Water Formation Occurs Primarily in the Iceland  
987 Basin and Irminger Sea by Local Buoyancy Forcing, *Geophys. Res. Lett.*, 47, 1–9, <https://doi.org/10.1029/2020GL091028>,  
988 2020.
- 989 Pickarski, N., Kwiecien, O., and Litt, T.: Volcanic impact on terrestrial and aquatic ecosystems in the Eastern Mediterranean,  
990 *Commun. Earth Environ.*, 4, 1–12, <https://doi.org/10.1038/s43247-023-00827-0>, 2023.
- 991 Pinta, E.: Norse Management of Wooden Resources across the North Atlantic: Highlights from the Norse Greenlandic  
992 Settlements, *Environ. Archaeol.*, 26, 209–221, <https://doi.org/10.1080/14614103.2018.1547510>, 2021.
- 993 Plucinski, M. P., Anderson, W. R., Bradstock, R. A., and Gill, A. M.: The initiation of fire spread in shrubland fuels recreated  
994 in the laboratory, *Int. J. Wildl. Fire*, 19, 512–520, <https://doi.org/10.1071/WF09038>, 2010.
- 995 Power, M. J., Marlon, J., Ortiz, N., Bartlein, P. J., Harrison, S. P., Mayle, F. E., Ballouche, A., Bradshaw, R. H. W., Carcaillet,  
996 C., Cordova, C., Mooney, S., Moreno, P. I., Prentice, I. C., Thonicke, K., Tinner, W., Whitlock, C., Zhang, Y., Zhao, Y., Ali,  
997 A. A., Anderson, R. S., Beer, R., Behling, H., Briles, C., Brown, K. J., Brunelle, A., Bush, M., Camill, P., Chu, G. Q., Clark,  
998 J., Colombaroli, D., Connor, S., Daniau, A. L., Daniels, M., Dodson, J., Doughty, E., Edwards, M. E., Finsinger, W., Foster,  
999 D., Frechette, J., Gaillard, M. J., Gavin, D. G., Gobet, E., Haberle, S., Hallett, D. J., Higuera, P., Hope, G., Horn, S., Inoue, J.,  
1000 Kaltenrieder, P., Kennedy, L., Kong, Z. C., Larsen, C., Long, C. J., Lynch, J., Lynch, E. A., McGlone, M., Meeks, S., Mensing,  
1001 S., Meyer, G., Minckley, T., Mohr, J., Nelson, D. M., New, J., Newnham, R., Noti, R., Oswald, W., Pierce, J., Richard, P. J.  
1002 H., Rowe, C., Sanchez Goñi, M. F., Shuman, B. N., Takahara, H., Toney, J., Turney, C., Urrego-Sanchez, D. H., Umbanhowar,  
1003 C., Vandergoes, M., Vanniere, B., Vescovi, E., Walsh, M., Wang, X., Williams, N., Wilmshurst, J., and Zhang, J. H.: Changes  
1004 in fire regimes since the last glacial maximum: An assessment based on a global synthesis and analysis of charcoal data, *Clim.*  
1005 *Dyn.*, 30, 887–907, <https://doi.org/10.1007/s00382-007-0334-x>, 2008.
- 1006 Prokopenko, A., Williams, D. F., Kavel, P., and Karabanov, E.: The organic indexes in the surface sediments of Lake Baikal  
1007 water system and the processes controlling their variation, *IPPCCE Newslett.*, 7, 49–55, 1993.
- 1008 Purushothama, S., Pan, W. P., Riley, J. T., and Lloyd, W. G.: Analysis of polynuclear aromatic hydrocarbons from coal fly  
1009 ash, *Fuel Process. Technol.*, 53, 235–242, [https://doi.org/10.1016/S0378-3820\(97\)00056-8](https://doi.org/10.1016/S0378-3820(97)00056-8), 1998.
- 1010 Quirk, M. M., Wardroper, A. M. K., Brooks, P. W., Wheatley, A. E., and Maxwell, J. R.: Transformations of acyclic and cyclic  
1011 isoprenoids in recent sedimentary environments, in: *Biogéochimie de la matière organique à l'interface eau-sédiment marin*.  
1012 Centre National de la Recherche Scientifique. Colloque international. 293/1979/Marseille; France; Paris: Ed. du CNRS; DA.,  
1013 225–232, PASCALGEODEBRGM8120323455, 1980.
- 1014 R Core Team: R: A Language and Environment for Statistical Computing. R Foundation for Statistical Computing, Vienna,  
1015 Austria., <https://www.r-project.org/>, 2020.
- 1016 Raposeiro, P. M., Hernández, A., Pla-rabes, S., Gonçalves, V., and Bao, R.: Climate change facilitated the early colonization  
1017 of the Azores Archipelago during medieval times, *Proc. Natl. Acad. Sci.*, 118, [https://doi.org/10.1073/pnas.2108236118/-](https://doi.org/10.1073/pnas.2108236118/-/DCSupplemental)  
1018 */DCSupplemental*.Published, 2021.
- 1019 Rein, G., Cleaver, N., Ashton, C., Pironi, P., and Torero, J. L.: The severity of smouldering peat fires and damage to the forest



- 1020 soil, *Catena*, 74, 304–309, <https://doi.org/10.1016/j.catena.2008.05.008>, 2008.
- 1021 Richter, N., Russell, J. M., Garfinkel, J., and Huang, Y.: Impacts of Norse settlement on terrestrial and aquatic ecosystems in  
1022 Southwest Iceland, *J. Paleolimnol.*, 65, 255–269, <https://doi.org/10.1007/s10933-020-00169-3>, 2021.
- 1023 Rieger, S., Schoepfoster, D. B., and Furbush, C. E.: Exploratory soil survey of Alaska, US Department of Agriculture, Soil  
1024 Conservation Service, 1979.
- 1025 Routh, J., Hugelius, G., Kuhry, P., Filley, T., Tillman, P. K., Becher, M., and Crill, P.: Multi-proxy study of soil organic matter  
1026 dynamics in permafrost peat deposits reveal vulnerability to climate change in the European Russian Arctic, *Chem. Geol.*, 368,  
1027 104–117, <https://doi.org/10.1016/j.chemgeo.2013.12.022>, 2014.
- 1028 Roy, N., Bhiry, N., Woollett, J., and Fréchette, B.: Vegetation History since the Mid-Holocene in Northeastern Iceland,  
1029 *Ecoscience*, 25, 109–123, <https://doi.org/10.1080/11956860.2018.1443419>, 2018.
- 1030 Rundel, P. W., Stichter, W., Zander, R. H., and Ziegler, H.: Carbon and hydrogen isotope ratios of bryophytes from arid and  
1031 humid regions, *Oecologia*, 44, 91–94, 1979.
- 1032 Sachse, D., Billault, I., Bowen, G. J., Chikaraishi, Y., Dawson, T. E., Feakins, S. J., Freeman, K. H., Magill, C. R., McNerney,  
1033 F. A., van der Meer, M. T. J., Polissar, P., Robins, R. J., Sachs, J. P., Schmidt, H., Sessions, A. L., White, J. W. C. C., West,  
1034 J. B., Kahmen, A., and Meer, M. T. J. Van Der: Molecular Paleohydrology: Interpreting the Hydrogen-Isotopic Composition  
1035 of Lipid Biomarkers from Photosynthesizing Organisms, *Annu. Rev. Earth Planet. Sci.*, 40, 221–249,  
1036 <https://doi.org/10.1146/annurev-earth-042711-105535>, 2012.
- 1037 Santana, V. M. and Marrs, R. H.: Flammability properties of British heathland and moorland vegetation: Models for predicting  
1038 fire ignition, *J. Environ. Manage.*, 139, 88–96, <https://doi.org/10.1016/j.jenvman.2014.02.027>, 2014.
- 1039 Santana, V. M., Baeza, M. J., and Vallejo, V. R.: Fuel structural traits modulating soil temperatures in different species patches  
1040 of Mediterranean Basin shrublands, *Int. J. Wildl. Fire*, 20, 668–677, <https://doi.org/10.1071/WF10083>, 2011.
- 1041 Scarff, F. R. and Westoby, M.: Leaf litter flammability in some semi-arid Australian woodlands, *Funct. Ecol.*, 20, 745–752,  
1042 <https://doi.org/10.1111/j.1365-2435.2006.01174.x>, 2006.
- 1043 De Schutter, A., Kervyn, M., Canters, F., Bosshard-Stadlin, S. A., Songo, M. A. M., and Mattsson, H. B.: Ash fall impact on  
1044 vegetation: a remote sensing approach of the Oldoinyo Lengai 2007–08 eruption, *J. Appl. Volcanol.*, 4, 1–18, 2015.
- 1045 Sear, D. A., Allen, M. S., Hassall, J. D., Maloney, A. E., Langdon, P. G., Morrison, A. E., Henderson, A. C. G., Mackay, H.,  
1046 Croudace, I. W., Clarke, C., Sachs, J. P., Macdonald, G., Chiverrell, R. C., Leng, M. J., Cisneros-Dozal, L. M., and Fonville,  
1047 T.: Human settlement of East Polynesia earlier, incremental, and coincident with prolonged South Pacific drought, *Proc. Natl.*  
1048 *Acad. Sci.*, 201920975, <https://doi.org/10.1073/pnas.1920975117>, 2020.
- 1049 Segato, D., Villoslada Hidalgo, M. D. C., Edwards, R., Barbaro, E., Vallelonga, P., Kjær, H. A., Simonsen, M., Vinther, B.,  
1050 Maffezzoli, N., Zangrando, R., Turetta, C., Battistel, D., Vésteinsson, O., Barbante, C., and Spolaor, A.: Five thousand years  
1051 of fire history in the high North Atlantic region: Natural variability and ancient human forcing, *Clim. Past*, 17, 1533–1545,  
1052 <https://doi.org/10.5194/cp-17-1533-2021>, 2021.
- 1053 Shillito, L.-M., Whelton, H. L., Blong, J. C., Jenkins, D. L., Connolly, T. J., and Bull, I. D.: Pre-Clovis occupation of the  
1054 Americas identified by human faecal biomarkers in coprolites from Paisley Caves, Oregon, *Sci. Adv.*, 1–9,  
1055 <https://doi.org/10.1126/sciadv.aba6404>, 2020.
- 1056 Siao, W. S., Balasubramanian, R., Rianawati, E., Karthikeyan, S., and Streets, D. G.: Characterization and source  
1057 apportionment of particulate matter  $\leq 2.5 \mu\text{m}$  in Sumatra, Indonesia, during a recent peat fire episode, *Environ. Sci. Technol.*,  
1058 41, 3488–3494, <https://doi.org/10.1021/es061943k>, 2007.
- 1059 Simpson, I. A., Van Bergen, P. F., Perret, V., Elhmmali, M. M., Roberts, D. J., and Evershed, R. P.: Lipid biomarkers of  
1060 manuring practice in relict anthropogenic soils, *Holocene*, 9, 223–229, <https://doi.org/10.1191/095968399666898333>, 1999.
- 1061 Sistiaga, A., Berna, F., Laursen, R., and Goldberg, P.: Steroidal biomarker analysis of a 14,000 years old putative human  
1062 coprolite from Paisley Cave, Oregon, *J. Archaeol. Sci.*, 41, 813–817, <https://doi.org/10.1016/j.jas.2013.10.016>, 2014.



- 1063 Slater, G. F., Benson, A. A., Marvin, C., and Muir, D.: PAH fluxes to Siskiwit revisited: Trends in fluxes and sources of  
1064 pyrogenic PAH and perylene constrained via radiocarbon analysis, *Environ. Sci. Technol.*, 47, 5066–5073,  
1065 <https://doi.org/10.1021/es400272z>, 2013.
- 1066 Smith, B. N. and Epstein, S.: Two Categories of  $^{13}\text{C}/^{12}\text{C}$  ratios for Higher Plants, *Plant Physiol.*, 47, 380–384,  
1067 <https://doi.org/10.1104/pp.47.3.380>, 1971.
- 1068 Smith, K. P.: Landnám: the settlement of Iceland in archaeological and historical perspective, *World Archaeol.*, 26, 319–347,  
1069 <https://doi.org/10.1080/00438243.1995.9980280>, 1995.
- 1070 Stein, A. F., Draxler, R. R., Rolph, G. D., Stunder, B. J. B., Cohen, M. D., and Ngan, F.: NOAA’s HYSPLIT atmospheric  
1071 transport and dispersion modeling system, *Bull. Am. Meteorol. Soc.*, 96, 2059–2077, <https://doi.org/10.1175/BAMS-D-14->  
1072 00110.1, 2015.
- 1073 Stogiannidis, E., Laane, R., and Broderick, G.: Source characterization of polycyclic aromatic hydrocarbons by using their  
1074 molecular indices: an overview of possibilities, *Rev. Environ. Contam. Toxicol.*, 234, 49–133, <https://doi.org/10.1007/978-3->  
1075 319-10638-0, 2015.
- 1076 Sugiyama, S., Minowa, M., Fukamachi, Y., Hata, S., Yamamoto, Y., Sauter, T., Schneider, C., and Schaefer, M.: Subglacial  
1077 discharge controls seasonal variations in the thermal structure of a glacial lake in Patagonia, *Nat. Commun.*, 12, 1–9,  
1078 <https://doi.org/10.1038/s41467-021-26578-0>, 2021.
- 1079 Sveinbjarnardóttir, G., Erlendsson, E., Vickers, K., McGovern, T. H., Milek, K. B., Edwards, K. J., Simpson, I. A., and Cook,  
1080 G.: The palaeoecology of a high status Icelandic farm, *Environ. Archaeol.*, 12, 187–206,  
1081 <https://doi.org/10.1179/174963107x226453>, 2007.
- 1082 Thomas, E. K., Briner, J. P., Ryan-Henry, J. J., and Huang, Y.: A major increase in winter snowfall during the middle Holocene  
1083 on western Greenland caused by reduced sea ice in Baffin Bay and the Labrador Sea, *Geophys. Res. Lett.*, 43, 5302–5308,  
1084 <https://doi.org/10.1002/2016GL068513>. Received, 2016.
- 1085 Thorarinsson, S.: The eruptions of Hekla in historical times. In: Einarsson, T., Kjartansson, G., Thorarinsson, S. (Eds.), *The*  
1086 *eruption of Hekla 1947–1948 I*, *Soc. Sci. Isl.*, Reykjavík, 1–177, 1967.
- 1087 Thorarinsson, S.: Vötnin stríð, *Saga Skeidarárhlaupa og Grímsvatnagosa* [The swift Flow. rivers Hist. Grímsvötn jökulhlaups  
1088 eruptions. Icelandic]. Menn. Reykjavík, 1974.
- 1089 Tierney, J. E., Pausata, F. S. R., and DeMenocal, P. B.: Rainfall regimes of the Green Sahara, *Sci. Adv.*, 3,  
1090 <https://doi.org/10.1126/sciadv.1601503>, 2017.
- 1091 Trouet, V., Esper, J., Graham, N. E., Baker, A., Scourse, J. D., and Frank, D. C.: Persistent Positive North Atlantic Oscillation  
1092 Mode Dominated the Medieval Climate Anomaly, *Science*, 324, 78–80, <https://doi.org/10.1126/science.1166349>, 2009.
- 1093 Tyagi, P., Edwards, D. R., and Coyne, M. S.: Fecal sterol and bile acid biomarkers: Runoff concentrations in animal waste-  
1094 amended pastures, *Water. Air. Soil Pollut.*, 198, 45–54, <https://doi.org/10.1007/s11270-008-9824-7>, 2009.
- 1095 Vachula, R. S., Huang, Y., Longo, W. M., Dee, S. G., Daniels, W. C., and Russell, J. M.: Evidence of Ice Age humans in  
1096 eastern Beringia suggests early migration to North America, *Quat. Sci. Rev.*, 205, 35–44,  
1097 <https://doi.org/10.1016/j.quascirev.2018.12.003>, 2019.
- 1098 Vachula, R. S., Huang, Y., Russell, J. M., Abbott, M. B., Finkenbinder, M. S., and O’Donnell, J. A.: Sedimentary biomarkers  
1099 reaffirm human impacts on northern Beringian ecosystems during the Last Glacial period, *Boreas*,  
1100 <https://doi.org/10.1111/bor.12449>, 2020.
- 1101 Vázquez, C., Vallejo, A., Vergès, J. M., and Barrio, R. J.: Livestock activity biomarkers: Estimating domestication and diet of  
1102 livestock in ancient samples, *J. Archaeol. Sci. Reports*, 40, 103220, <https://doi.org/10.1016/j.jasrep.2021.103220>, 2021.
- 1103 Wallace, J. M. and Hobbs, P. V.: *Atmospheric science: an introductory survey*, Academic Press, ISBN 0-12-732951-X, 2006.
- 1104 Wang, Q. and Huang, H.: Perylene preservation in an oxidizing paleoenvironment and its limitation as a redox proxy,  
1105 *Palaeogeogr. Palaeoclimatol. Palaeoecol.*, 562, <https://doi.org/10.1016/j.palaeo.2020.110104>, 2021.



- 1106 Wardroper, A. M. K., Maxwell, J. R., and Morris, R. J.: Sterols of a diatomaceous ooze from walvis bay, *Steroids*, 32, 203–  
1107 221, [https://doi.org/10.1016/0039-128X\(78\)90006-5](https://doi.org/10.1016/0039-128X(78)90006-5), 1978.
- 1108 Wilkie, K. M. K., Chaplignin, B., Meyer, H., Burns, S., Petsch, S., and Brigham-Grette, J.: Modern isotope hydrology and  
1109 controls on  $\delta D$  of plant leaf waxes at Lake El'gygytgyn, NE Russia, *Clim. Past*, 9, 335–352, [https://doi.org/10.5194/cp-9-335-](https://doi.org/10.5194/cp-9-335-2013)  
1110 2013, 2013.
- 1111 Wooller, M., Wang, Y., and Axford, Y.: A multiple stable isotope record of Late Quaternary limnological changes and  
1112 chironomid paleoecology from northeastern Iceland, *J. Paleolimnol.*, 40, 63–77, <https://doi.org/10.1007/s10933-007-9144-8>,  
1113 2008.
- 1114 Landmælingar Íslands: <https://www.lmi.is/is/moya/page/licence-for-national-land-survey-of-iceland-free-data>, last access: 1  
1115 March 2023.
- 1116 Icelandic Meteorological Office: [www.vedur.is](http://www.vedur.is), last access: 1 January 2022.
- 1117 Yunker, M. B., Macdonald, R. W., Vingarzan, R., Mitchell, H., Goyette, D., and Sylvestre, S.: PAHs in the Fraser River basin:  
1118 a critical appraisal of PAH ratios as indicators of PAH source and composition, *Org. Geochem.*, 33, 489–515,  
1119 [https://doi.org/10.1016/S0146-6380\(02\)00002-5](https://doi.org/10.1016/S0146-6380(02)00002-5), 2002.
- 1120 Zennaro, P., Kehrwald, N., McConnell, J. R., Schüpbach, S., Maselli, O. J., Marlon, J., Vallelonga, P., Leuenberger, D.,  
1121 Zangrando, R., Spolaor, A., Borrotti, M., Barbaro, E., Gambaro, A., and Barbante, C.: Fire in ice: Two millennia of boreal  
1122 forest fire history from the Greenland NEEM ice core, *Clim. Past*, 10, 1905–1924, <https://doi.org/10.5194/cp-10-1905-2014>,  
1123 2014.
- 1124 Zennaro, P., Kehrwald, N., Marlon, J., Ruddiman, W. F., Brücher, T., Agostinelli, C., Dahl-Jensen, D., Zangrando, R.,  
1125 Gambaro, A., and Barbante, C.: Europe on fire three thousand years ago: Arson or climate?, *Geophys. Res. Lett.*, 42, 5023–  
1126 2033, <https://doi.org/10.1002/2015GL064259>, 2015.
- 1127